A molecular dynamics study of the nonlinear spectra and structure of charged (101) quartz/water interfaces

Konstantin Smirnov

A molecular dynamics study of nonlinear spectra and structure of charged (101) quartz/water interface†

Konstantin S. Smirnov

Univ. Lille, CNRS, UMR 8516 – LASIRe – Laboratoire Avancé de Spectroscopie pour les Interactions la Réactivité et l'Environnement, F-59000 Lille, France

E-mail: konstantin.smirnov@univ-lille.fr

The relation between the nonlinear spectra and the structure of charged (101) α-quartz/water interface was investigated by classical molecular dynamics. The results of the simulations show that the layered organization of interfacial water is only slightly perturbed by the surface charge and the ionic strength of the aqueous phase. Molecules next to the surface, in bonded interfacial layer (BIL), tend to direct one of their OH bonds towards the surface, while the water orientation further from the surface, in diffuse layer (DL), is essentially isotropic. A Stern layer of solvated cations is built up already on a neutral surface and the deprotonation of silanols leads to the formation of an inner Helmholtz plane of cations directly interacting with the SiO^- surface sites. A flip of the molecular orientation in DL could be inferred from analysis of the structural characteristics of concentrated NaCl solution in contact with highly charged surface. Computed spectra of $\chi^{(2)}$ susceptibility show a double band structure typical of spectra of silica/water interfaces and the calculations reproduce the experimentally observed variation of the spectral intensity with the pH of the liquid phase. The analysis of results suggests that the behaviour stems from interplay between orientational and induced components of the $\chi^{(2)}$ susceptibility of BIL and DL. The dependence of $\mathrm{Im}[\chi^{(2)}]$ spectra of BIL on the surface charge yields the spectrum of H_2O molecules directly interacting with the SiO^- sites. The spectrum is in an excellent agreement with the experimental spectrum of topmost water of silica/water interface [Urashima et al. **J. Phys. Chem. Lett.**, 2018, 9, 4109].

1 Introduction

Silica and water are two most abundant compounds in the Earth's mantle and physico-chemical processes at the frontier of these two substances are of paramount importance to geochemistry, heterogeneous chemistry of atmosphere, catalysis, biomedical applications of silica[1,2]. While the knowledge on the structure and dynamics of water in the interfacial region at the microscopic level underpins understanding the mechanisms of surface phenomena, a very low surface-to-bulk ratio and the buried character of the silica/water interfaces impede obtaining this information. The difficulty can be overcome by using surface-specific experimental techniques, such as atomic force microscopy[3], X-ray reflectivity[4], and the second-harmonic generation (SHG) and vibrational sum-frequency generation (VSFG) nonlinear spectroscopy[5–8]. The nonlinear spectroscopy can selectively probe the interfacial region because, in electric dipole approximation, the second-order optical processes become active due to the inversion symmetry broken at the interface[9,10]. In particular, the VSFG spectroscopy permits to determine the magnitude of the second-order nonlinear susceptibility $\chi^{(2)}$ as a function of the IR beam frequency and the vibrational resonances in the $\chi^{(2)}$ spectrum are indicative of species present in the interfacial region. Furthermore, phase-sensitive (heterodyne-detected) VSFG can provide information about the orientation of molecules on the surface from the analysis of sign of the imaginary part of the complex $\chi^{(2)}$ quantity. Results of experimental studies of mineral/water interfaces, and silica/water one in particular, by the SHG and VSFG methods has been reviewed by Backus and co-workers[11]. Outcome of

†Electronic Supplementary Information (ESI) available: Parameters of interatomic interaction potentials; details on computation of structural characteristics and nonlinear spectra; complementary sets of results.

time-resolved VSFG investigations of the systems is presented in a very recent review article by Piontek and Borguet[12].

As the point of zero charge (PZC) of silica surface corresponds to pH 2–3 of aqueous phase[1], increasing pH above the PZC conditions leads to the deprotonation of surface hydroxy groups and the surface becomes negatively charged. Structure of interfacial region of a charged solid/liquid interface is commonly discussed in terms of Gouy-Chapman-Stern-Grahame electrical double layer (EDL) model[13–15]. In this model, a region near the surface with thickness of a few molecular sizes is referred to as Stern layer (SL). This compact layer of water molecules and ions with their hydration shell is characterized by surface-specific bonding network. The ions demarcate the so-called outer Helmholtz plane. Besides, some ions can directly interact with charged surface sites and they form the inner Helmholtz plane. The outer Helmholtz plane marks the onset of a diffuse or Gouy-Chapman layer (DL), where water and solvated ions have a bulk-like structure, yet perturbed by surface electric field. The spatial extent of the DL is commonly characterized by the Debye screening length which is inversely proportional to the ion concentration.

The effect of pH of liquid phase on the VSFG spectra of silica/water interfaces has been addressed in many experimental studies[5,16–26]. A typical VSFG intensity spectrum of the interface in the ssp polarization combination features two broad bands at about 3200 cm^{-1} and 3400 cm^{-1} and phase-sensitive VSFG experiments showed that the bands have the negative and positive sign in the $Im[\chi^{(2)}]$ spectra, respectively, at a neutral pH value[18,19]. Already the first VSFG investigation of the system revealed a change of the relative intensities of the bands in the spectra with pH and the finding was interpreted as an order-disorder phase transition accompanied by a flip of molecular orientation[16]. The phase-sensitive VSFG study of quartz/water interface by Shen and co-workers showed an influence of pH on the amplitudes of the 3200 cm^{-1} and 3400 cm^{-1} bands and the low-frequency band was found to change its sign from negative to positive at pH of about 6–7[18]. The behaviour was associated with the existence of surface silanols with different deprotonation pK values[18]. Borguet and co-workers investigated the effect of electrolyte on ssp VSFG signal for a range of pH from 2 to 12 and obtained that the nonlinear response most changed at a neutral pH value[20]. The authors explained the results by a higher disorder of molecular arrangement induced by solvated cations at the neutral pH conditions. Gibbs et al.[21,22] considered silica/water interface at pH from 2 to 12 for 0.1 M and 0.5 M ionic strengths of NaCl solution, and analysed VSFG spectra with different polarization settings in the experimental setup. The intensity of VSFG signal in the pss polarization combination was found to increase monotonically with pH, whereas the intensity of ssp VSFG signal had a minimum near a neutral pH value[22]. Results of the study were related to the presence of two water regions having a distinct pH-dependent behavior and the authors attributed the 3200 cm^{-1} band to molecules in the DL, whereas the band at 3400 cm^{-1} was ascribed to water in the SL. This interpretation supported the conclusion of an earlier study by Jena and Hore[27]. The authors of ref. 22 proposed two scenarios to explain the pH dependence of the VSFG spectra. The first scenario considered the effect of overcharging of Stern layer on the orientation of molecules in the SL and DL, while the second one evoked a distortion of solvation shell around cations in the SL. Tahara and co-workers investigated silica/isotopically diluted water interface with a phase-sensitive VSFG experimental setup, and found that the $Im[\chi^{(2)}]$ spectrum with the negative low-frequency negative and positive high-frequency bands at neutral pH changed to a totally positive signal at pH of 12[19]. The effect was explained by a pH-dependent water orientation at the interface and in particular, by a net H-up orientation of water molecules at the high pH value. More recently, the same group studied the silica/water interface at pH 12 in a wide range of ionic strengths[23]. Using the dependence of Debye screening length on the ion concentration, the authors could separate the spectrum of the topmost water molecules from that of DL. The $Im[\chi^{(2)}]$ spectrum of the molecules had an intense positive band at 3200 cm^{-1} and a weak negative band at 3500 cm^{-1} that were ascribed

to water with OH bonds directed to the O^- atom of silanolate and to the liquid phase, respectively. It was concluded that such molecules are the dominant species in the SL at high pH. A combined experimental and computational study by Tuladhar et al.[25] showed that a major contribution to the VSFG signal at pH > 6 and moderate electrolyte concentrations comes from the DL region, whereas an information specific to SL can be obtained by analysing the nonlinear spectra at low pH values and high ionic concentrations. The authors concluded that adsorption of monovalent cations on the surface as inner-sphere complexes has a kosmotropic effect on water in the topmost layer and affects the surface hydrophobicity.

Summarizing, the experimental studies show a complex dependence of the nonlinear response on pH of liquid phase that is commonly interpreted as a result of co-existance of two interfacial regions with distinct spectral patterns and different response to pH change. A scenario often proposed from the analysis of the VSFG data is a flip of molecular orientation around a neutral pH value, although other possibilities could not be ruled out, such as overcharging of the SL and/or distortion of hydration shells of cations. Yet the mechanisms behind the pH-dependence of VSFG spectra remain dim.

Molecular dynamics (MD) simulation method is a powerful and versatile tool for understanding the behavior of complex systems at the molecular level. Outcome of both classical and ab initio MD studies of water on surfaces of solids and of silica in particular, has been reviewed in refs. 28–30. A number of modeling works addressed the formation and characteristics of EDL on silica surfaces[31–36]. The timescale of MD simulations nicely matches that probed by vibrational spectroscopies and in the two recent decades, the technique has been widely applied to modelling nonlinear spectra of a number of interfacial systems[25,33,37–48]. Using MD simulation results, Pezzotti et al.[45] have suggested a structural definition of different regions of solid/liquid interfaces. They have defined the first layer of water in the immediate proximity to the surface as bonded interfacial layer (BIL) and a more distant than BIL region with the intermolecular structure similar to that of bulk water, was related to a diffuse layer. The authors pointed to that BIL corresponds to the SL for charged surfaces, whereas the spectroscopic diffuse layer is a reoriented part of the DL of the EDL theory[45,49]. Subsequent works by the same group analyzed BIL and DL contributions to VSFG spectra of silica/water interface[46,47]. For water on the (001) α-quartz and amorphous silica surfaces, the authors assigned a positive band at 3400 cm^{-1} in $Im[\chi^{(2)}]$ spectra to BIL water molecules, while a negative band at 3200 cm^{-1} was attributed to water in the diffuse layer, in line with the assignment proposed in refs. 21,22,27. In contrast to the result by Tuladhar and co-workers[25], the inner-sphere KCl electrolyte complexes were obtained to have a chaotropic effect on bonding in BIL. Analysis of the $Im[\chi^{(2)}]$ spectra of DL showed that the spectra provide a wealth of information on interfacial properties, such as surface potential and surface charge, EDL formation[46].

Most of the MD simulation studies dealt with the computation of VSFG spectra of silica/water interfaces employed electronic-structure theory methods, mainly based on DFT, for computing the interatomic energies and forces[25,45–47]. However, the high expenditures of such calculations strongly limit the size of studied systems, sampling time and the accessible range of electrolyte concentrations. On the other hand, MD simulations using effective potentials permit to obtain nonlinear spectra of significantly bigger systems for much longer trajectories and thus, with an improved statistical sampling[43,50–54]. Thus, a recent classical MD study of several neutral silica/water interfaces has shown that the $Im[\chi^{(2)}]$ spectrum of BIL features both the negative 3200 cm^{-1} and positive 3400 cm^{-1} bands with a surface-specific shape of the latter[54]. No notable effect of ions on the bonding in BIL and on the nonlinear spectra was revealed. The DL spectrum was obtained to have a shape similar for all systems with a band at 3200 cm^{-1} which interferes with the BIL band in this wavenumber range. In agreement with the results by Pezzotti et al.[46], the DL spectrum was obtained to be dominated by a contribution from the third-order $\chi^{(3)}$ susceptibility with the sign related to that of electrostatic potential at the outer

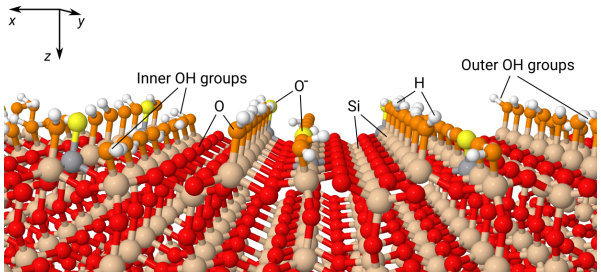

Figure 1: A view of the (101) surface of α-quartz. Color legend: red – oxygen of siloxane bridges, orange – oxygen of silanol groups, yellow – oxygen of SiO^- groups, peach - Q_3 and Q_4 silicon atoms, gray – silicon atoms of SiO^- groups, white - hydrogens. The two types of the vicinal OH groups are indicated.

Helmholtz plane. However, despite the valuable information provided by the previous MD simulations of the system, no systematic computational investigation of the influence of surface charge (bulk pH) and electrolyte concentration on the relation between the nonlinear spectra and structural organization of a well characterized silica/water interface has been performed yet.

The present work aims at bridging the gap and reports results of classical molecular dynamics study of the structure and nonlinear $\chi^{(2)}$ spectra of NaCl solution in contact with the (101) surface of α-quartz for a series of pH values and for two ionic strengths of the liquid phase. Change of pH of bulk water is mimicked by deprotonation of surface OH groups and in this way, the surface charge density is varied from zero corresponding to bulk pH of 2–3 to values typical for silica in contact with a basic solution with pH of about 9. The choice of the (101) surface ($(10\bar{1}1)$ in the Miller-Bravais notation) is explained by the fact that it is the most stable of hydroxylated low-index α-quartz surfaces[55] and the surface has the density of surface OH groups close to that typical of silica[56] Moreover, the (101) surface is one of three most common faces (the "r" face) of natural quartz crystals[57]. The work has considered two electrolyte concentration of 0.25 M and 0.5 M. It is worthy of noting that the latter concentration is close to that in sea water and thus, some models can be viewed as an archetype of silica/water interface present in nature. The main goals of the work are (i) to study the effect of surface charge on the structure, bonding and nonlinear spectra of the system and (ii) to suggest a microscopic interpretation of experimental VSFG results by analysing outcome of the atomistic simulations.

2 Models and Methods

The molecular dynamics simulations were performed in a slit-pore layout, where the liquid phase was confined between two (101) surfaces of α-quartz. The surface has a density of hydroxy groups of 5.6 OH/nm^2 and it features two types of vicinal silanols with the oxygen atoms of outer OH groups by 0.76 Å more lifted above the surface than the atoms of inner hydroxyls, Figure 1. The silica layer had dimensions of 41.274 Å and 39.306 Å along the x and y axes, respectively, and a thickness of 24.16 Å. Initially, the distance between the two surfaces was set to 38 Å and the interlayer void was filled with H_2O molecules with a density slightly smaller than the density of bulk liquid water. Then, the size of simulation box in the z-direction was adjusted so that the density in the center of the interlayer space attained the density of bulk water. The procedure has resulted in an MD box with two silica surfaces distant by 36.4 Å measured as difference of z-coordinates of oxygen atoms of the outer OH groups on the opposite surfaces.

Five silica surfaces with charge densities of 0.00, -0.12, -0.37, -0.62 and -0.86 $|e|/nm^2$ were considered in the work. The charged surfaces were obtained by removing H atoms of surface hydroxy groups in a random way under two constraints. First, both surfaces had to possess the same number of SiO^- groups. Second, the groups on each surface had to be separated by a distance greater than

Table 1: Nominal pH value of liquid phase, surface charge density σ, number of SiO^- groups, silanols deprotonation ratio, number of Na^+ ions, number of water molecules and total number of atoms in the systems.

Nominal pH	3	6	7	8	9
σ, $\lvert e\rvert$/nm^2	0.0	−0.12	−0.37	−0.62	−0.86
No. SiO^- groups	0	4	12	20	28
Deprotonation ratio, %	0.0	2.1	6.2	10.4	14.6
No. Na^+ ions[a]	9/18	13/22	21/30	29/38	37/46
No. H_2O molecules	1902/1884	1898/1880	1890/1872	1882/1864	1874/1856
Total No. atoms	9036/9000	9024/8988	9000/8964	8976/8940	8952/8916

[a] The first and the second entry correspond to the ionic strength of 0.25 M and 0.5 M, respectively.

$\sqrt{S/\pi N^-}$, where S and N^- are the surface area and the number of deprotonated hydroxyls on the surface, respectively[58]. The negative surface charge was compensated by extra cations added into the aqueous phase as described below. The neutral (fully hydroxylated) silica surface corresponds to the PZC condition and the nominal pH value of 3 was assigned to the system. The charged surfaces can be related to silica/water interfaces at bulk water pH approximately equal to 6, 7, 8 and 9, respectively[59–61]. Note that these values are round-off estimates of aqueous phase pH for the above surface charge densities. Since surface charge directly correlates with pH value of liquid phase, these properties will be used interchangeably throughout the paper. Additional calculations were performed for the neutral surface in contact with neat water.

The electrolyte solution was obtained by a random substitution of water molecules with Na^+ and Cl^- ions so that (i) no two ions could be found at a distance smaller than 5.6 Å (2nd minimum in O–O RDF), and (ii) the initial ion-surface distance along the z-axis was greater than the radius of the first solvation shell, *i.e.* the ions could have a complete shell at $t = 0$. In this way, electrolyte solutions with ionic strengths of 0.25 M and 0.5 M were prepared for each charged surface. In what follows, each system will often be identified by the nominal pH value and the electrolyte concentration, *e.g.* pH3@0.25M for the neutral silica surface in contact with the 0.25 M NaCl solution. Table 1 reports a pertinent information on the systems.

Water molecules were represented with the SPCFw water model[53,62]. The interactions between the molecules and silica atoms were described with the INTERFACE force field[63] with a slight modification. It turned out that the use of the original INTERFACE parameters for the O^- atom of SiO^- groups in combination with the flexible water model gave rise to a system instability. The reason was that the O^- atom could tear a hydrogen of a nearby H_2O molecule that produced a sudden raise of energy and the system "exploded". To avoid the undesirable breaking of O-H bonds, van der Waals parameters of O^- were set to those of the SPC oxygen that can be justified by similar charges of the two atoms[64]. Parameters for the Na^+ and Cl^- ions were taken from ref. 65. The Lorentz-Berthelot combining rules were used to compute van der Waals parameters for unlike atoms. Parameters of interatomic potentials are given in Table S1†.

The molecular dynamics simulations were carried out for a temperature of 293 K and results presented below are the averages of 50 runs for each pH value and each ionic strength. A single run consisted of an equilibration stage of 30 ps in an NVT ensemble followed by a 50 ps NVE step. The coordinates and velocities of atoms were stored each 4 fs for the last 40 ps of the NVE stage. The final configuration of each run was used as the starting configuration for the subsequent one, whereas the atomic velocities in each run were freshly chosen from the Maxwell-Boltzmann distribution. Prior to performing the series of production runs, the systems were equilibrated at $T = 293$ K for 10 ns. In the simulations, the H atoms of the surface hydroxy groups were allowed to move, while the other atoms of silica were kept fixed at their initial positions. As in ref. 54, the mass of the silanol H atoms was set to

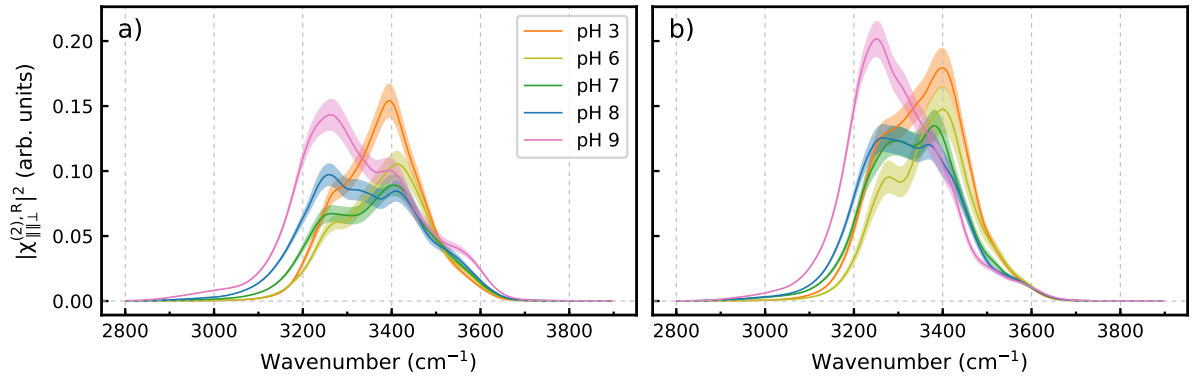

Figure 2: $|\chi^{(2),R}_{|||\perp}|^2$ spectra of (101) α-quartz/water interface at different pH values for 0.25 M (**a**) and 0.5 M (**b**) ionic strengths. Colored areas represent the standard error.

the mass of deuterium. Most of experimental information is extracted from the analysis of VSFG spectra in the ssp polarization combination. Such spectrum in the work is obtained as an average of spectra of the xxz and yyz elements of the resonant part of $\chi^{(2)}$ tensor and the quantity is denoted as $\chi^{(2),R}_{|||\perp}$ throughout the paper. Details on the computation of structural descriptors and of the second-order nonlinear susceptibility are provided ESI†.

3 Results and discussion

3.1 Nonlinear spectra of quartz/water interface

3.1.1 Intensity spectra

The calculated $|\chi^{(2),R}_{|||\perp}|^2$ spectra of the systems are displayed in Figure 2. The spectra reveal a typical double band pattern observed in the ssp VSFG spectra of silica/water interfaces[16–22,26,27,66]. The high-frequency and low-frequency bands have been initially ascribed to H_2O molecules forming liquid-like and ice-like structures on the surface, respectively, whereas the change of relative intensities of the bands upon variation of pH has been related to an order-disorder transition in the interfacial water layer[16–18]. Subsequently, it was suggested that the high-frequency (liquid-like) band stems from molecules next to the surface, whereas the low-frequency (ice-like) one is due to molecules in a more distant from the surface region[27]. Recently, the interpretation was questioned by results of isotopic dilution experiments that showed the absence of the double band in the spectra of silica/HOD–D_2O interface[19]. Based on this result, the authors of ref. 19 explained the double band by intramolecular and/or intermolecular vibrational coupling. However, the latter interpretation cannot account for a different dependence of the band intensities on pH value and on electrolyte concentration[21,22,26,27].

The classical water model employed in the present calculations lacks the intramolecular coupling mechanism that is the $\nu_{OH}/2\delta_{OH}$ Fermi resonance and with this respect, the calculations better correspond to the isotopic dilution experiments in ref. 19. Yet the computed spectra reveal the low-frequency and high-frequency bands. On the other hand, the intermolecular coupling is included in both the MD simulations and the computation of the nonlinear susceptibility (see section **??** and SI). A recent modeling study of water/air interface showed that the intermolecular coupling was essential for reproducing the experimental VSFG spectra of that system[67]. Therefore, this mechanism cannot be completely ruled out as the origin of the double band structure in Figure 2, although it is unlikely that it plays an important role†.

Another notable feature of ssp VSFG spectra of silica/water interface is a non-monotonic behav-

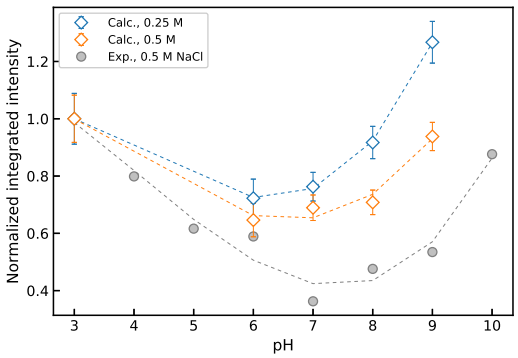

Figure 3: Integrated intensity of the $|\chi^{(2),R}_{|||\perp}|^2$ spectrum as a function of pH value. Gray filled circles show experimental results for amorphous silica/0.5 M NaCl solution interface[22]. The data in each set were normalized for the intensity value at pH 3. Dashed lines to guide the eye.

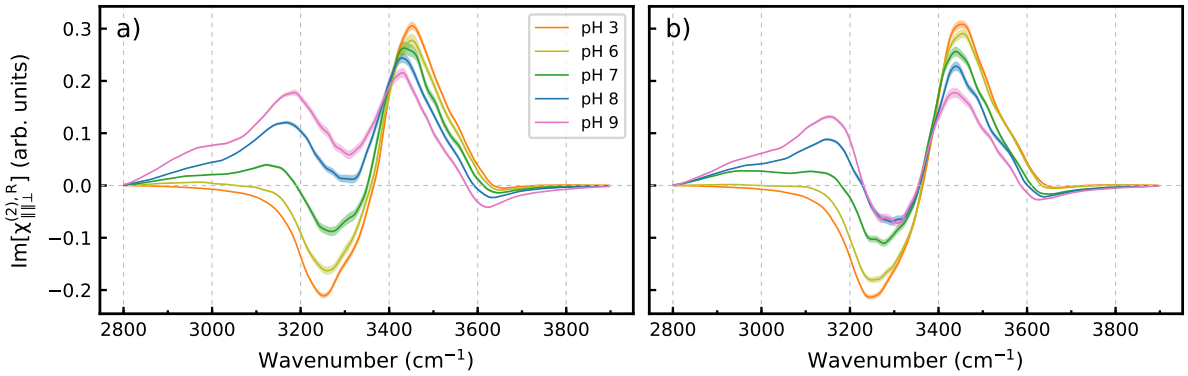

Figure 4: Im$[\chi^{(2),R}_{|||\perp}]$ spectra of BIL as a function of pH value for the 0.25 M (**a**) and 0.5 M (**b**) NaCl solutions. Colored areas represent the standard error.

ior of the spectral intensity with change of pH[21,22,24]. Figure 3 presents dependence of the integrated intensity in the calculated $|\chi^{(2),R}_{|||\perp}|^2$ spectra on the pH value, and compares the dependence with the experimental trend[22]. One sees that the results of the calculations are in line with the observation. The intensity vs pH graph has a minimum at around neutral pH value. The feature has been explained by a flip of molecular orientation at these conditions[16,19,22]. An interpretation of the behavior of the $\chi^{(2),R}_{|||\perp}$ intensity spectra will be provided below, after discussing results of the calculations of phase-sensitive nonlinear spectra of the system. In the following, the layer of interfacial water next to the surface is referred to as BIL[45] while a region extending by 7 Å from BIL to the bulk part of the liquid phase corresponds to DL[54] (see Section 3.2 for more detail).

3.1.2 Im$[\chi^{(2)}]$ spectra of BIL

The calculated Im$[\chi^{(2),R}_{|||\perp}]$ spectra of BIL as a function of pH are shown in Figure 4. The spectra behave similarly for both the electrolyte concentrations. For the neutral surface/water interface at pH 3, the spectrum is characterized by a positive band at 3450 cm^{-1} and a negative band at 3250 cm^{-1} that are assigned to OH oscillators directed towards the surface and liquid phase, respectively. When the surface becomes negatively charged, intensity of the bands decreases and a new positive band at about 3180 cm^{-1} starts to grow and attenuates the negative band at 3250 cm^{-1}. At high pH values this new band gives a major contribution to the spectrum below 3300 cm^{-1}, Figure 4.

Analysis of the series of the spectra in Figure 4 reveals the presence of an isobestic point at *ca.* 3400

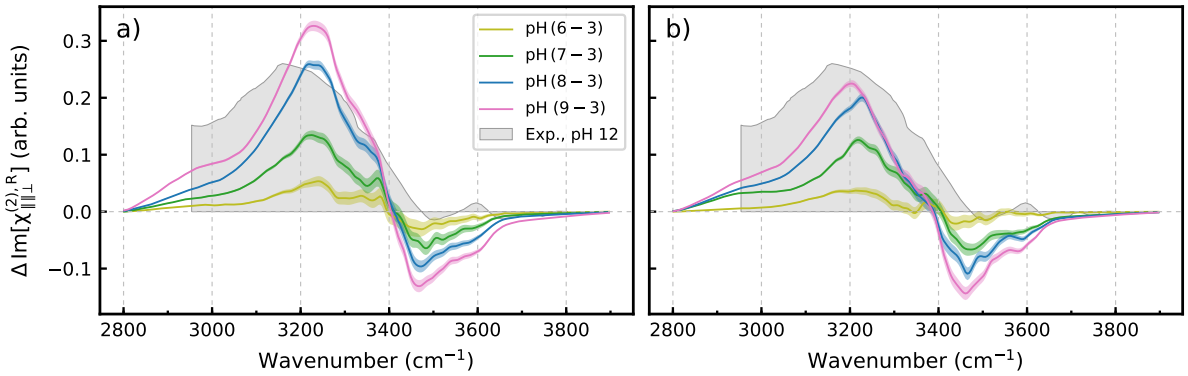

Figure 5: Difference of the Im$[\chi^{(2),R}_{|||\perp}]$ spectra of BIL (pH (# – 3), # = 6, 7, 8, 9) for the 0.25 M (**a**) and 0.5 M (**b**) NaCl solutions; colored areas represent standard error. The shadowed spectrum shows the experimental Im$[\chi^{(2)}_{ssp}]$ spectrum of the topmost water layer on amorphous silica surface; the spectrum was digitized from Figure 2b of ref. 23. Colored areas represent the standard error.

cm^{-1} that implies a co-existence of two types of water in BIL. Assuming that molecules of first type are at the origin of the spectrum at pH 3, one can retrieve a spectrum of second water type by taking the difference between the spectrum at a particular value of pH and that at pH 3. The so-obtained spectra are displayed in Figure 5. Clearly, the spectra belong to the same species whose concentration grows with increase of pH value. This second type of water can be related to molecules interacting with the SiO^- surface groups and involved in an asymmetric H-bonding. One H atom of such molecules strongly interacts with the deprotonated oxygen and the corresponding weak OH bond yields the positive band at about 3200 cm^{-1}, whereas the second bond is essentially directed to the liquid phase and yields the negative signal at 3450 cm^{-1}, Figure 5.

The spectrum of the second type of H_2O molecules can be compared with the experimental spectrum of topmost water on surface of fused silica[23] shown by a shadowed spectrum in Figure 5. One sees a very good agreement between the result of the calculations and the experimental spectrum. Authors of ref. 23 have assigned the principal positive band at 3200 cm^{-1} to molecules donating one of their hydrogens to SiO^- sites and the other H atom to different H-bond accepting sites. The interpretation is fully consistent with the result of the present work. The result is also in line with the outcome of a recent MD study of phase-resolved VSFG spectrum of ice/water interface[68]. The spectrum of the system was found to have a distinct signature, strongly resembling the spectra in Figure 5, which was assigned to water involved in an asymmetric H-bonding with molecules of the solid and liquid phases.

3.1.3 Im$[\chi^{(2)}]$ spectra of DL.

Figure 6 displays the calculated Im$[\chi^{(2),R}_{|||\perp}]$ spectra of diffuse layer as a function of pH for the two electrolyte concentrations. At the 0.25 M concentration the increase of pH from 3 to 6–7 does not strongly affect the spectrum that is characterized by a positive band at 3250 cm^{-1} and a negative band at about 3400 cm^{-1}. At more basic conditions the former band almost disappears while the latter increases in intensity, Figure 6a. At the higher ionic strength the DL spectrum features a wide negative band already at pH 3 and the band monotonically grows in intensity when pH increases, Figure 6b. Regardless the salt concentration, the DL spectra are dominated by the negative signal from 3200 to 3600 cm^{-1} at high values of pH. It is noteworthy that the position of minimum of the negative band depends on the concentration. Results presented in the following section shed a light on the origin of the DL spectra behaviour.

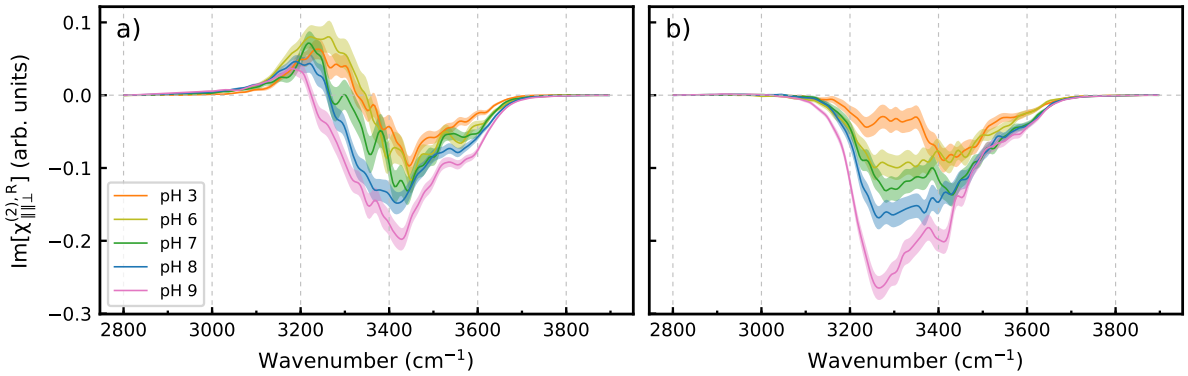

Figure 6: Im[$\chi^{(2),R}_{|||\perp}$] spectra of DL as a function of pH value for the 0.25 M (**a**) and 0.5 M (**b**) NaCl solutions. Colored areas represent the standard error.

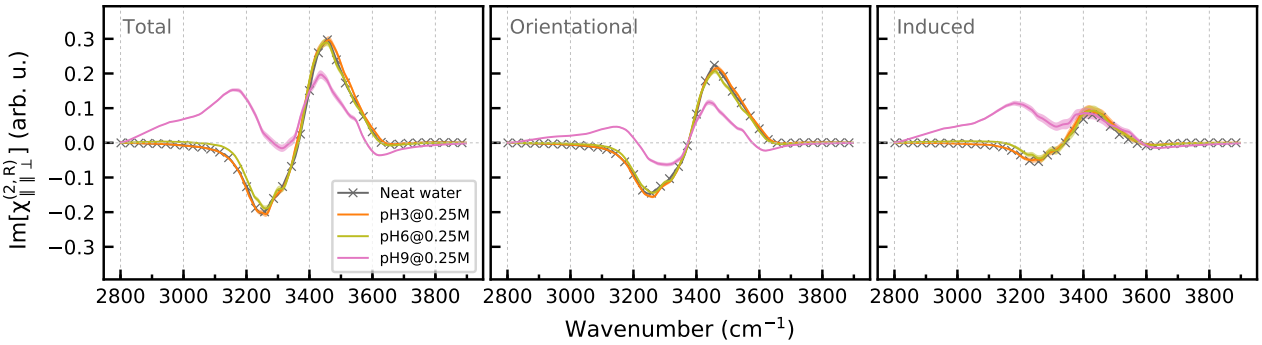

Figure 7: Breakdown of the Im[$\chi^{(2),R}_{|||\perp}$] spectra of BIL on (101) α-quartz/water interfaces at the 0.25 M electrolyte concentration into the orientational and induced components. The corresponding spectra of neutral surface/neat water interface are given for completeness. Colored areas represent the standard error.

3.1.4 Orientational and induced components of Im[$\chi^{(2)}$] spectra

The nonlinear response of interfacial region is due to the lack of inversion symmetry at the frontier between two media[9,10] and, for a charged surface, one can distinguish two contributions to the $\chi^{(2)}$ susceptibility of interfacial water layer. The first contribution results from an orientational ordering of molecules because of molecule-surface interactions. The second one is related to an anisotropy of molecular polarization due to the interfacial electric field. Relative importance of these two contributions depends on the surface characteristics, distance from the surface and composition of aqueous phase. Thus, the orientational term is expected to play a major role in the immediate proximity to the surface, while the induced term prevails in a more distant region where the orientation of molecules is (almost) isotropic.

In the present work, the orientational and induced components of $\chi^{(2),R}$ susceptibility were computed separately that has allowed the analysis of their contributions to the nonlinear susceptibility of different interfacial regions, and of their variation with surface charge. The breakdown of Im[$\chi^{(2),R}_{|||\perp}$] spectra of BIL on the quartz/water interfaces for the 0.25 M ionic strength into the two components is shown in Figure 7. For the sake of completeness, the figure also displays such a breakdown for the spectrum of a neutral quartz surface/neat water interface.

Figure 7 reveals that neither orientational nor induced components of BIL spectrum depend on surface charge below pH of 6, and the spectra almost coincide with counterparts obtained for the neutral surface/neat water interface, Figure 7. Increasing pH above this threshold leads to an overall decrease

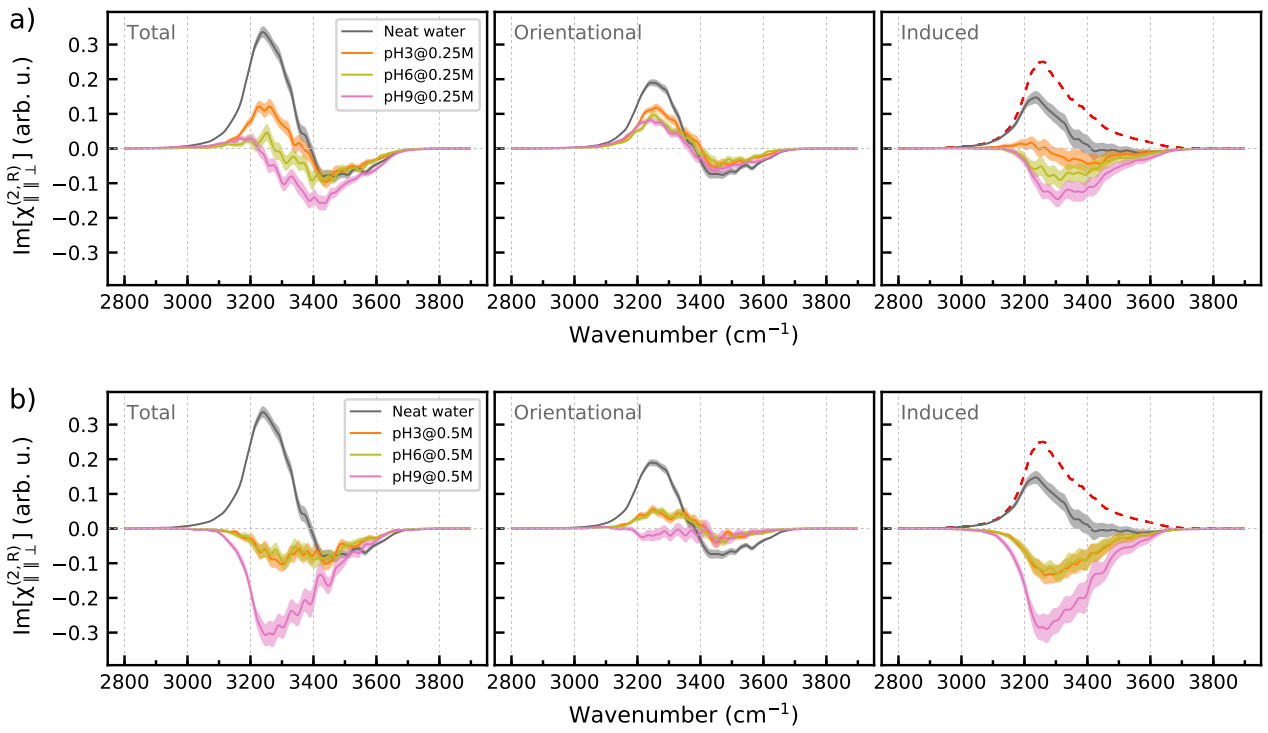

Figure 8: Breakdown of the Im[$\chi^{(2),R}_{\parallel\parallel\perp}$] spectra of DL on (101) α-quartz/water interfaces into the orientational and induced components at the 0.25 M (**a**) and 0.5 M (**b**) electrolyte concentrations. The corresponding spectra of neutral surface/neat water interface are given for completeness. Colored areas represent the standard error. Red dashed line in the right-hand panels shows calculated $\chi^{(3),R}_{\parallel\parallel\perp\perp}$ spectrum of bulk water.

of the intensity in the spectrum of the orientational component and to growth of a new positive band at about 3180 cm^{-1}. As discussed above, the band is related to the molecules interacting with the SiO^- sites, while the decrease of the intensity can presumably be ascribed to an effect of Na^+ ions in the layer. Regarding the induced component, the increase of negative surface charge results in a change of sign of the low-frequency part of the induced spectrum. This positive band at 3180 cm^{-1} in the spectrum of the induced component is readily explained by the polarization of the OH bonds binding by their H atom up to the negative surface sites. The sum of both the components accounts for the intense positive band at 3180 cm^{-1} in the BIL spectrum at high pH values (Figure 4). The components of BIL spectrum for the 0.5 M salt concentration behave similarly†.

Figure 8 presents the breakdown of DL spectra. One sees that an intense positive band at about 3250 cm^{-1} in the DL spectrum of a neutral surface/neat water interface arises from the sum of both orientational and induced components, whereas only the orientational component explains a negative band at *ca.* 3450 cm^{-1}. The intensity of the component is reduced when salt is added to water in contact with the neutral surface. At the 0.25 M electrolyte concentration, Figure 8a, the orientational component is not affected by the surface charge that implies that the orientational ordering of water in DL remains unaffected by pH change. At the 0.5 M electrolyte concentration, Figure 8b, the spectrum of orientational component does not depend on pH for pH < 6, but the spectral intensity becomes slightly negative at a pH value of 9 (integrated intensity is equal to -6.6 ± 5.6). This finding implies a change of molecular orientation in DL of NaCl solution with the higher salt concentration in contact with a highly charged silica surface. It is worthy of noting the smaller intensity of the component for systems with the 0.5 M ionic strength that points to a more isotropic structure of DL in solution with higher electrolyte concentration. The dependence of the orientational component on the ionic strength

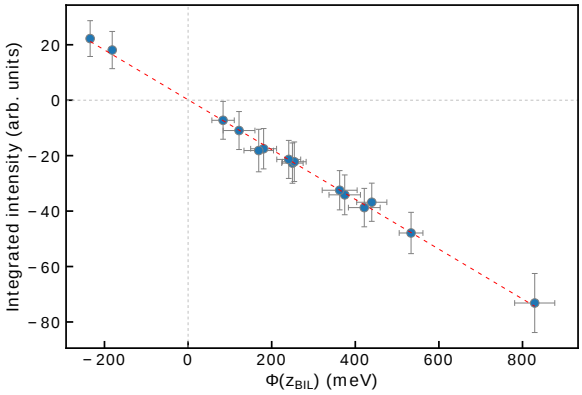

Figure 9: Dependence of integrated intensity of the induced component of $\chi^{(2)}$ susceptibility of the DL on electric potential $\Phi(z_{BIL})$. The red dashed line shows a linear regression fit of the calculated data.

explains the variation of the position of minimum of the negative band in the DL spectra, Figure 6 and Figure 8b.

The $\mathrm{Im}[\chi^{(2),R}_{|||\perp}]$ spectrum of the induced component behave with pH similarly for the two electrolyte concentration, Figure 8. The spectrum reverses its sign upon adding ions into the liquid phase and the intensity of the corresponding negative band grows with increase of surface charge. This induced component of DL spectrum, $\chi^{(2),\mathrm{ind}}_{DL}$, can be identified as the $\chi^{(3)}$ term which was shown to be of importance for rationalizing the VSFG spectra of charged solid/water interfaces[5,43,46,49,54,69]. Then, $\chi^{(2),\mathrm{ind}}_{DL}$ is related to the third-order susceptibility of bulk as[5,43,49]

$$\chi^{(2),\mathrm{ind}}_{DL} = -\chi^{(3)}_{B}\Phi(z_{BIL}), \tag{1}$$

where $\chi^{(3)}_{B}$ and $\Phi(z_{BIL})$ are the third-order susceptibility of bulk liquid water and electric potential at the frontier between the DL and BIL, respectively. The right-hand panels in Figure 8 compares the spectra of the induced component with a computed $\chi^{(3),R}_{|||\perp\perp}$ spectrum of bulk water† and shows a good agreement between the spectra. Furthermore, if the relation (1) holds, the integrated intensity of the induced spectrum should be proportional to the potential $\Phi(z_{BIL})$. Figure 9 displays a graph of the intensity as a function of $\Phi(z_{BIL})$ value[70]. There is indeed a linear correlation between the quantities with a correlation coefficient better than 0.998 and a linear fit passing through the origin. A similar linear relation between the intensity of DL spectrum and the electric potential was previously obtained by Pezzotti et al.[46], although their calculated spectra were not broken down into the two components. The result was likely due to a small contribution of the orientational component to the total intensity because of the sine-like shape of the component's spectrum, Figure 8.

3.1.5 Spectra reproducibility.

Figure 10 displays $\mathrm{Im}[\chi^{(2),R}_{|||\perp}]$ spectra obtained for the pH6@0.25M system in four series of 50 runs. The spectrum of BIL (Figure 10a) remains essentially unchanged from one series to another as well as the high frequency part of the DL spectrum (Figure 10b). As it was discussed above, the latter results from the orientational component of $\chi^{(2)}_{DL}$ susceptibility. On the other hand, the low frequency part of the DL spectrum partly due to the induced component shows a disparity with series of simulations. As a result, the corresponding part of spectrum of the entire interfacial region (Figure 10c) also varies between different series, yet the spectra behave qualitatively similar. Anticipating the following presentation, the spectra variation below 3400 cm^{-1} can be related to a different density of cations in BIL. The result indicates the need of a good sampling for a statistically sound $\chi^{(2)}$ spectra of charged solid/water

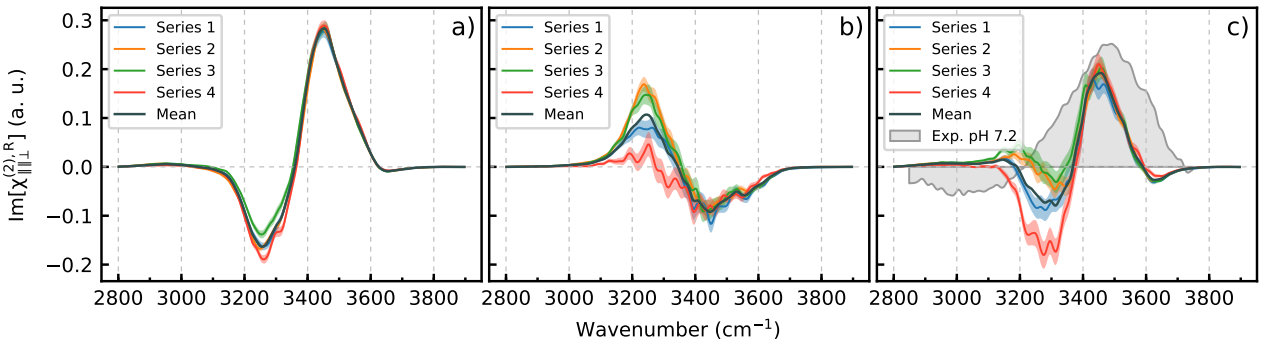

Figure 10: Im$[\chi^{(2),R}_{|||\perp}]$ spectra of pH6@0.25M system computed in four series of simulations: (**a**) – BIL spectra, (**b**) – DL spectra; (**c**) – total spectra of the interface. Experimental Im$[\chi^{(2)}_{ssp}]$ spectrum of amorphous silica/HOD-D_2O interface at pH 7.2 is shown as shadowed gray spectrum in panel (**c**); the spectrum was digitized from Fig. 3a of ref. 19.

interface.

Figure 10c also compares the calculated total spectra with experimental ssp Im$[\chi^{(2)}_{|||\perp}]$ spectrum of silica/isotopically diluted water interface measured at pH 7.2[19]. One observes a good qualitative agreement, whereas differences in the position and shape of bands in the spectra can be ascribed to limitations of the classical water model that does not take into account such effects as the increase of transition dipole moment of OH oscillator upon the H-bond formation and the charge transfer along H-bonds[71,72].

3.1.6 Outline of spectroscopic results

The results presented above clearly demonstrate the importance of considering the signed BIL and DL contributions to account for the nonlinear spectra of silica/water interface. Each contribution includes orientational and induced components that interfere over entire OH frequency range. At surface charge densities corresponding to pH < 6, the BIL spectrum essentially remains unchanged and this behaviour of the spectrum is to a large extent independent of the ionic strength of liquid phase. Regarding the DL spectrum, its orientational component does not vary with pH for the lower electrolyte concentration and at the higher ionic strength for pH < 6. At the higher ionic strength and a high pH value, the spectrum of the component points to an eventual flip of molecular orientation. The induced component of DL spectrum is completely determined by the $\chi^{(3)}$ bulk susceptibility and depends on the sign and magnitude of surface electric potential.

The results shed light on the observed features in the VSFG spectra of silica/water interface. Thus, the interplay between the BIL and DL contributions and their components accounts for the variation of relative intensities of the low- and high-frequency bands in the VSFG spectra with pH. Furthermore, below pH 6 the spectral changes are primarily due to a change of the induced component of DL spectrum. Close to neutral pH values, the induced component nearly cancels the orientational one in a low-frequency region, Figure 8, that accounts for the minimum in the dependence of the VSFG intensity on pH (Figure 3). This finding also suggests that the spectrum at pH∼6 mainly reflects that of BIL, in agreement with conclusion by Tuladhar et al.[25]. Above the neutral pH value, changes of the total spectrum stem from the interplay between the two components of BIL spectrum and the induced component of DL spectrum which grows in intensity with increase of pH value.

The analysis of the computed spectra permits to obtain the following information about the effect of pH on the structure of silica/water interface. In bonded interfacial layer, increase of pH accompanied by deprotonation of surface OH groups leads to the appearance of a new water population. Molecules

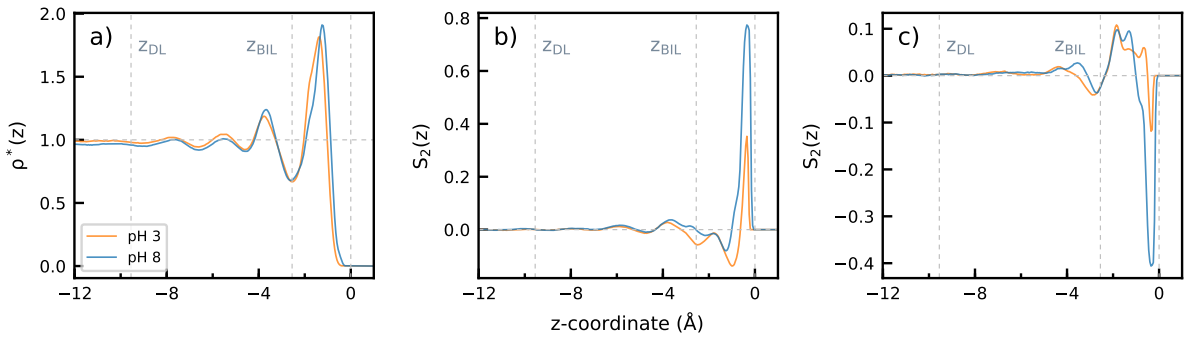

Figure 11: Axial profiles of the relative density $\rho^*(z)^\dagger$ (**a**) and of the order parameters $S_2(z)^\dagger$ for the dipole (**b**) and HH vector (**c**) of H_2O molecules in the pH3@0.25M (orange line) and pH8@0.25M (blue line) systems. The origin of the z-axis is placed at the position of topmost oxygen atoms of the surface and the vertical dashed lines labeled z_{BIL} and z_{DL} indicate limits of BIL and DL, respectively.

of this new type interact with surface SiO^- sites and are involved in an asymmetric H-bonding. In diffuse layer, a net orientational ordering of water exists already at PZC conditions. The orientation is not affected by increase of pH at a low electrolyte concentration, whereas the ordering can be altered for a concentrated salt solution in contact with a highly charged surface. These conclusions will now be compared to information extracted from the analysis of structural descriptors.

3.2 Structure and bonding in the interfacial region

3.2.1 Structural characteristics

Figure 11a displays profile of the relative density $\rho^*(z)$ (S2) of water molecules in the interlayer space of the pH3@0.25M and pH8@0.25M systems. Analysis of the profiles shows that the presence of negative SiO^- sites on the surface and of solvated ions in the liquid phase does not notably affect the layered water structure. Yet one can notice a small shift of the first density peak accompanied by a slight increase of its intensity. Figure 11 shows that thickness of BIL defined as the z-coordinate of the first minimum in the $\rho^*(z)$ profile and labelled as z_{BIL}, is independent of the surface charge. The mean number density of water in BIL remains virtually the same for all systems and is equal to $\rho_{BIL} = 29.3 \pm 0.6\ \mathrm{nm}^{-3}$ that is slightly smaller than the density of water in the bulk ($33.4\ \mathrm{nm}^{-3}$). Further from the surface, one finds diffuse layer which is associated with a region extending to 7 Å beyond the BIL; the DL limit is marked by z_{DL} in Figure 11. Previously, it was found that the spacial extent of the DL is largely insensitive to characteristics of silica surfaces, such as density of surface OH groups or surface morphology[54].

Figure 11b and Figure 11c display profiles of the orientation order parameter S_2 (S3) for the molecular dipole and the HH vector, respectively, in the two systems. In contrast to $\rho^*(z)$ weakly perturbed by the surface charge, the S_2 profiles show a significant effect of the negative SiO^- sites on the orientation of H_2O molecules in the first water layer. From the analysis of the order parameters, it follows that some molecules in BIL on the charged silica surface adapt an orientation with their dipole and the HH vector parallel and perpendicular to the surface normal, respectively. On the other hand, orientational ordering of molecules in the DL is influenced by the surface charge to a much lesser extent.

Further insight into the orientation of water molecules in BIL and DL and its dependence on the surface charge can be obtained from the inspection of the $\widetilde{P}(u_1, u_2, \mathcal{Z})$ maps (S6), Figure 12 and Figure 13. Molecules in BIL are oriented with at least one OH bond towards the surface, as suggested by $\widetilde{P} < 1$ values in the $(u_1 < 0, u_2 < 0)$ quadrant, Figure 12. The presence of negatively charged sites on the surface at pH > 3 leads to a marked increase of probability to find molecules with two OH bonds

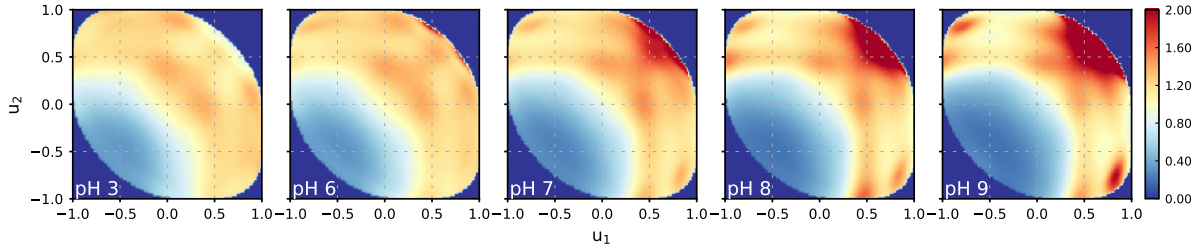

Figure 12: $\widetilde{P}(u_1, u_2, \mathcal{Z})$ maps† for H_2O molecules in BIL of the (101) α-quartz/water interface at different pH values for the 0.25 M electrolyte concentration.

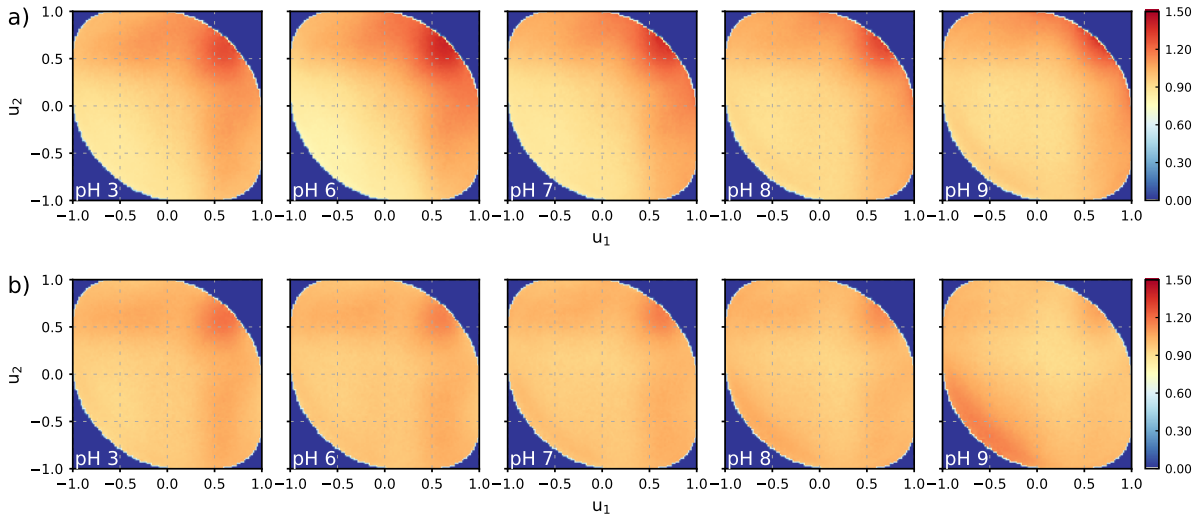

Figure 13: $\widetilde{P}(u_1, u_2, \mathcal{Z})$ maps† for H_2O molecules in DL of the (101) α-quartz/water interface at different pH values for the 0.25 M (**a**) and 0.5 M (**b**) electrolyte concentrations.

directed to the surface. The molecular dipole and the HH vector of such molecules are nearly parallel and perpendicular to the z-axis, respectively, that agrees with the behaviour of the S_2 order parameters in BIL upon charging the surface, Figure 11b,c. Furthermore, the evolution of the maps in Figure 12 due to the H_2O molecules interacting with SiO^- surface groups is consistent with the spectra of such molecules in Figure 5 and with the behaviour of the orientational component of the BIL spectrum in Figure 7.

Contrarily, the orientation of water in diffuse layer is significantly more isotropic than in BIL, Figure 13. Yet at the lower electrolyte concentration, a preferred orientation of molecules with at least one OH bond directed to the surface can be deduced from the analysis of the maps in Figure 13a. The $\widetilde{P}(u_1, u_2, BIL)$ maps computed for the higher ionic strength reveal a similar, although less intense, pattern for pH < 9, Figure 13b. Such smaller contrast in the maps correlates with a reduced intensity of the orientational component of the DL spectrum at the higher ionic strength, Figure 8. The $\widetilde{P}(u_1, u_2, DL)$ map for pH 9 in Figure 13b features $\widetilde{P} > 1$ values in the $(u_1 < 0, u_2 < 0)$ quadrant that implies that the diffuse layer now has water molecules with a preferred orientation with two OH bonds directed towards the liquid phase. The map is in line with a slightly negative orientational component of the DL spectrum for the pH9@0.5M system in Figure 8b.

The examination of the structural descriptors presented above shows that the layered water structure in the interfacial region and the thickness of the bonded interfacial layer of molecules are to a large extent independent of the surface charge and the ionic strength of the electrolyte solution. Water molecules in BIL prefer to direct at least one of their OH bonds towards the surface and the negative

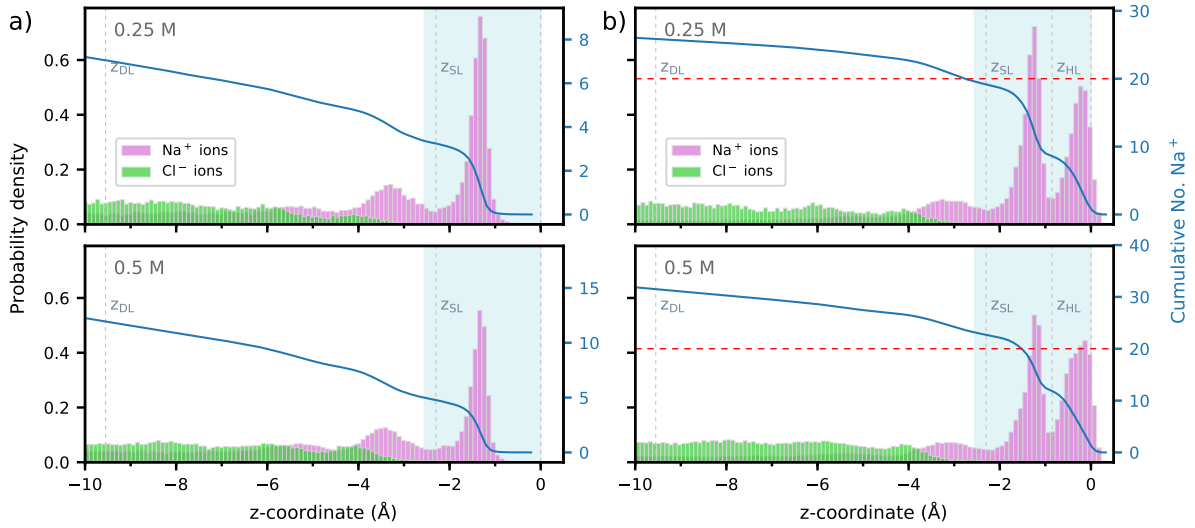

Figure 14: Histogram of ions distribution along the z-axis in the (101) quartz/water systems at pH 3 (**a**) and pH 8 (**b**) for two electrolyte concentrations. The dashed vertical lines labeled z_{DL}, z_{SL} and z_{HL} indicate limits of the diffuse layer (DL), Stern layer (SL) and Helmholtz layer (HL), respectively, and the shaded light blue zone denotes BIL. The right-hand ordinate axis and blue line correspond to a cumulative number of cations as a function of distance from the surface. The red dashed line in the graphs (**b**) indicates a number of cations needed to compensate a surface charge of -20$|e|$ at pH 8.

surface charge increases the probability to find BIL molecules with two OH bonds pointed to the surface. The molecules interact with the negative SiO^- surface sites. Orientation of H_2O molecules in the DL is significantly more isotropic than in BIL. The orientation of water in DL is not affected by increasing the surface charge for 0.25 M electrolyte concentration, whereas a flip of molecular orientation can be inferred for molecules in DL of a highly charged quartz/0.5 M NaCl solution interface. The results support the conclusions obtained from the analysis of computed nonlinear spectra.

3.2.2 Ions distribution

Figure 14 presents distributions of ions along the z-axis in the liquid phase in contact with the neutral and charged surfaces for two values of pH and of ionic strength. Similarly to water density, the Na^+ distributions have a layered profile. For the neutral surface, the first peak in the distributions is found at a distance of *ca.* 1.3 Å from the surface, Figure 14a. The cations are adsorbed as inner-sphere complexes and the adsorption form agrees with results of previous modeling studies[25,31,47,73]. An estimation based on the computed running coordination numbers of the cations in the bulk electrolyte and in the quartz/water systems at pH 3 gives *ca.* 4.2 H_2O molecules in the first hydration shell of the adsorbed Na^+ ions and the value is in line with the results by Pfeiffer-Laplaud and Gaigeot[73]. The loss of molecules in the solvation shell upon adsorption is in part compensated by the interaction with surface OH groups. In contrast to the distribution of cations, that of Cl^- co-ions is more homogeneous and the region close to the surface is depleted of the anions[35], Figure 14. No chlorine anions can be found within BIL even for the neutral surface.

The layer of the adsorbed Na^+ ions with water molecules of their hydration shell can be associated with the Stern layer of the EDL theory and the minimum between the first and second maxima in the Na^+ distribution demarcates the frontier between the SL and DL; the corresponding z-coordinate is marked as z_{SL} in Figure 14. From the comparison of Figure 11a and Figure 14, one sees that the SL is essentially identical to BIL of water molecules. Deprotonation of surface silanols leads to the formation of an additional layer of adsorbed cations at a distance of *ca.* 0.15 Å from the surface, Figure 14b.

Table 2: The surface density of cations θ in the SL and HL compared to the surface charge density σ for the systems.

	pH 3	pH 6	pH 7	pH 8	pH 9
σ, $\lvert e\rvert$/nm^2	0.0	-0.12	-0.37	-0.62	-0.86
θ_{SL}[a], Na$^+$/nm^2	0.10 (0.04)[b]	0.20 (0.04)	0.35 (0.04)	0.61 (0.06)	0.80 (0.04)
	0.16 (0.04)	0.28 (0.05)	0.48 (0.06)	0.72 (0.04)	1.01 (0.04)
θ_{HL}, Na$^+$/nm^2	0.00 (0.00)	0.05 (0.02)	0.16 (0.02)	0.27 (0.04)	0.35 (0.04)
	0.00 (0.00)	0.08 (0.02)	0.17 (0.03)	0.37 (0.06)	0.59 (0.11)

[a] The first and the second line correspond to the ionic strength of 0.25 M and 0.5 M, respectively.
[b] Values in parentheses are the standard errors.

As the layer is formed only on the surface possessing negative sites, one can attribute it to sodium ions interacting with the SiO^- groups. The layer can be regarded as the inner Helmholtz plane and thickness of the corresponding inner Helmholtz layer (HL) is defined by the minimum in the Na^+ distribution labelled by z_{HL} in Figure 14b. Analysis of Figure 14 shows that the spatial extent of the SL and HL is independent of either the surface charge or ionic strength in the range of values studied in the work. The thickness of the SL is approximately equal to 2.4 Å that reasonably agrees with a value of 2.6 Å obtained by extrapolating results of ref. 61 to the ionic strength 0.25 M.

Table 2 compares the surface charge density σ and the density of cations θ in the SL and HL of the systems. Taking θ_{SL} at pH 3 as an offset of the intrinsic negative surface charge, Figure 14b and Table 2 show that the ion density in the SL at the 0.25 M ionic strength is smaller than σ. The cation density in the SL grows with increase of salt concentration and the offset θ_{SL} at the 0.5 M ionic strength approximately equals to the negative surface charge. A similar increase the concentration of cations in the SL with the ionic strength was found for amorphous silica surface by Bouhadja and Skelton[34]. The density of Na^+ ions in the HL is always smaller than σ, regardless the electrolyte concentration that implies that the ions in the HL cannot completely dislodge water molecules bound to the negative sites. The result is in line with the conclusion by Tahara and co-workers[23] based on the persistence of the OH signal in the VSFG spectra of silica water/interface due to the topmost water molecules at high electrolyte concentrations. The calculations show that each SiO^- group binds in average with 2.4 BIL H_2O molecules and has about 0.7 Na cation at a distance corresponding to the first hydration shell. Considering the cation density in the SL of neutral surface, no overcharging of the SL can be inferred for the results presented in Figure 14 and Table 2.

The data reported in Table 2 for the pH6@0.25M system are those of the first series of calculations (see section 3.1.5). Values of θ_{SL} obtained for the series 2, 3 and 4 are equal to 0.17 ± 0.04, 0.14 ± 0.04 and 0.24 ± 0.05 Na^+/nm^2, respectively. Although these values are equal to each other within the statistical uncertainties and correspond to less than one Na^+ ion per area of 400 Å^2, such a small variation of the ion concentration in SL is clearly discernible in the Im[$\chi^{(2)}$] spectra in Figure 10b,c. Once more, the finding points to the importance of sampling for the quantitative modeling of the nonlinear spectra of charged solid/water interface.

3.2.3 H-bond network

Table 2 reports an H-bond analysis for water molecules in the systems. As it could be expected, charging the surface does not essentially influences number of intermolecular bonds in the DL and bulk parts of the liquid phase. Increasing the electrolyte concentration slightly reduces the number of H-bonds in these regions that is readily explained by the formation of solvation shell around the ions. In the BIL region, the total number of H-bonds per molecule is smaller than in the DL and bulk already at the PZC conditions. The growth of negative surface charge leads to decreasing the number of intermolecular

Table 3: Number of H-bonds per water molecule in the BIL, DL and bulk (BLK) regions, see Fig. 11 for the region definition. H-bonds in BIL are classified by donor – acceptor pair (D−A).

D−A pair	pH 3	pH 6	pH 7	pH 8	pH 9
Ow−Ow[a]	2.30/2.25	2.31/2.24	2.16/2.14	2.01/2.08	2.00/1.99
Ow−Oh	0.60/0.60	0.58/0.57	0.53/0.52	0.49/0.47	0.44/0.43
Oh−Ow	0.41/0.41	0.39/0.39	0.36/0.36	0.35/0.33	0.32/0.31
Ow−Ob	0.02/0.02	0.03/0.02	0.04/0.04	0.04/0.04	0.06/0.05
Ow−O^-		0.04/0.04	0.13/0.12	0.22/0.18	0.29/0.24
No. HB (BIL)	3.33/3.28	3.35/3.26	3.22/3.18	3.11/3.10	3.11/3.02
No. HB (DL)	3.42/3.36	3.42/3.36	3.40/3.34	3.38/3.30	3.36/3.33
No. HB (BLK)	3.43/3.36	3.41/3.35	3.41/3.34	3.41/3.35	3.40/3.35

[a] The first and the second entry correspond to the ionic strength of 0.25 M and 0.5 M, respectively.

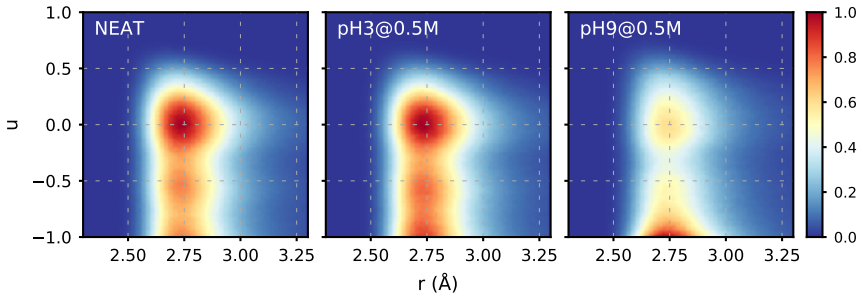

Figure 15: Two-dimensional maps of $Q(r,u,BIL)$ distribution† computed for the (101) α-quartz surface in contact with neat water and for the pH3@0.5M and pH9@0.5M systems. The distributions were normalized to a maximum value of the $Q(r,u,BIL)$ distribution of the quartz/neat water interface.

and water–silanol H-bonds and the total number of H-bonds for BIL molecules tends to diminish with the increase of pH. This behaviour can be related to the effect of Na^+ ions whose concentration in the SL increases with pH. The formation of solvation shell disrupts the H-bonding network in the layer, whereas newly formed bonds between H_2O molecules and the SiO^- groups cannot compensate the broken water–water and water–silanol contacts.

Figure 15 shows maps of joint probability distribution $Q(r,u,\mathcal{Z})$ (S7) of donor-acceptor vectors of intermolecular H-bonds in BIL of three systems chosen to illustrate the effect of ions. One sees that adding the electrolyte into the liquid phase in contact with a neutral surface has a little impact on the intermolecular bonding. In contrast, charging the surface strongly perturbs the H-bonds network in the layer that can be attributed to a combined action by adsorbed cations and negative surface sites, in line with data in Table 2. Therefore, increase of negative surface charge and, to a lesser extent, of ionic strength has a chaotropic effect on intermolecular H-bonding network in the BIL and DL regions of interface. A similar effect of K^+ ions on H-bonding in BIL was obtained by Pezzotti et al.[47] Although a spectroscopic identification of bonding changes in BIL could perhaps be performed by analysing the 3400 cm^{-1} band in the $\chi^{(2)}$ spectra, the value of such analysis would be uncertain as the band also has a contribution from the orientation component of DL spectrum.

4 Conclusions

An extensive MD simulation study with varying surface charge density and electrolyte concentration, was carried out to unveil the relation between the nonlinear spectra and the structure of water on charged (101) quartz surface. The calculated intensity spectra of the $\chi^{(2)}$ nonlinear susceptibility are

in a good agreement with the experimental VSFG spectra of silica/water interfaces and the calculated dependence of the spectral signal on the pH of the liquid phase closely follows the observed behaviour. The analysis of the spectral response as a function of distance from the surface shows that molecules of both BIL and DL of interfacial water contribute to the high-frequency and low-frequency bands in the spectra at 3400 and 3200 cm^{-1}, respectively, although the dependence of the contributions on the surface charge is different. Breaking the $\chi^{(2)}$ susceptibility down into orientational and induced components sheds light on the origin of spectral features. Thus, the BIL spectrum components were found to remain unaffected by the surface charge below a value corresponding to a neutral pH. Increasing the surface charge (bulk pH) above the threshold leads to the appearance of a new positive band at about 3180 cm^{-1} in the Im[$\chi^{(2)}$] spectrum. The comparison of the spectroscopic and structural information permits to assign this band to the OH bonds of water molecules interacting with the SiO^- groups and involved in an asymmetric H-bonding. The computed spectrum of such molecules is in an excellent agreement with the phase-sensitive VSFG spectrum of the topmost water on the amorphous silica surface[23]. Regarding DL spectrum, its change with pH arises from the induced component, the $\chi^{(3)}$ term, which depends on the sign and magnitude of surface electric potential[5,24,43,46,49]. The orientational component of the DL spectrum remains to a large extent unaffected by surface charge at low electrolyte concentration that points to the absence of change of the molecular orientation. However, a flip of the molecular orientation in DL of concentrated salt solution is evidenced for a highly charged silica surface.

The calculations show that the layered structure of interfacial water and the thickness of BIL are only slightly affected by the surface charge and ionic strength of the aqueous phase. Water molecules in BIL direct at least one of their OH bonds towards the surface and the deprotonation of surface OH groups enhances the probability of finding molecules with two bonds pointing to the surface. The orientation of H_2O molecules in DL is significantly more isotropic than in BIL and it is not affected by the surface charge at low electrolyte concentration. In agreement with the analysis of the DL spectra, a change of molecular orientation at a high pH value and a high electrolyte concentration could be inferred from the analysis of structural descriptors. Increasing the surface charge and salt concentration has a chaotropic effect on the H-bonding network in the interfacial water and the interactions of molecules with the SiO^- groups do not compensate the broken water–water and water–silanol hydrogen bonds. A Stern layer of cations is already formed on a neutral silica surface and the layer can be confidently associated with BIL of water. The Na^+ ions are adsorbed as inner-sphere complexes and the number of ions in the SL grows with increase of both surface charge and electrolyte concentration. A layer of cations directly interacting with the negative SiO^- sites builds up upon the deprotonation of surface silanols and this layer can be viewed as the inner Helmholtz plane. The balance between the surface charge and number of ions in the Stern layer plays the major role for water polarization in DL and determines the nonlinear spectrum of the layer.

The results of the study allows to propose a consistent explanation of the effect of the pH of the liquid phase on the nonlinear spectra of silica/water interface. The spectral changes can be interpreted as a result of interplay between the signed BIL and DL contributions to the $\chi^{(2)}$ susceptibility. While the double band structure in the spectra originates from the entire layer of interfacial water, different dependence of the BIL and DL contributions on the surface charge accounts for the variation of the relative intensities of the bands with pH value. At low pH values, spectral changes are mainly due to the DL contribution that changes its sign at a nearly neutral pH value and then steadily grows in intensity with increase of pH. The minimum in the dependence of the VSFG signal vs pH at pH $\sim 6-7$ results from the fact that the orientational and induced components of the DL spectrum almost cancel each other at such conditions. This result implies that the VSFG spectrum at the neutral pH essentially reflects the spectrum of BIL, especially at a high electrolyte concentration when the Debye screening length becomes comparable with the thickness of BIL. At higher pH values the interaction of BIL water

molecules with the negative SiO^- surface sites affect both orientational and induced components of the BIL spectrum. The dependence of both BIL and DL contributions on pH at basic conditions makes the interpretation of the nonlinear spectrum of the silica/water interface less certain, except for high pH values when the spectrum is dominated by a signal from H_2O molecules binding to the negative surface sites.

Acknowledgments

The author is grateful to Prof. Daniel Bougeard for critical reading the manuscript.

Conflicts of interest

There are no conflicts to declare.

References

[1] R. K. Iler. **The Chemistry of Silica**. John Wiley & Sons, Inc., New York, Chichester, Brisbane, Toronto, 2nd edition, 1979.

[2] E. Papirer. **Adsorption on Silica Surfaces**. Taylor & Francis, New York, 2000.

[3] S. P. Jarvis, T. Uchihashi, T. Ishida, H. Tokumoto, and Y. Nakayama. *Local solvation shell measurement in water using a carbon nanotube probe*. **J. Phys. Chem. B**, 2000, 104, 6091–6094, doi:10.1021/jp001616d.

[4] S. A. de Vries, P. Goedtkindt, S. L. Bennett, W. J. Huisman, M. J. Zwanenburg, D.-M. Smilgies, J. J. De Yoreo, W. J. P. van Enckevort, P. Bennema, and E. Vlieg. *Surface atomic structure of KDP crystals in aqueous solution: An explanation of the growth shape*. **Phys. Rev. Lett.**, 1998, 80, 2229–2232, doi:10.1103/PhysRevLett.80.2229.

[5] S. Ong, X. Zhao, and K. B. Eisenthal. *Polarization of water molecules at a charged interface: second harmonic studies of the silica/water interface*. **Chem. Phys. Lett.**, 1992, 191, 327–335, doi:https://doi.org/10.1016/0009-2614(92)85309-X.

[6] C. D. Bain. *Sum-frequency vibrational spectroscopy of the solid/liquid interface*. **J. Chem. Soc., Faraday Trans.**, 1995, 91, 1281–1296, doi:10.1039/FT9959101281.

[7] C. S. Tian and Y. R. Shen. *Recent progress on sum-frequency spectroscopy*. **Surf. Sci. Rep.**, 2014, 69, 105–131, doi:10.1016/j.surfrep.2014.05.001.

[8] P. E. Ohno, H. Chang, A. P. Spencer, Y. Liu, M. D. Boamah, H.-f. Wang, and F. M. Geiger. *Beyond the Gouy-Chapman model with heterodyne-detected second harmonic generation*. **J. Phys. Chem. Lett.**, 2019, 10, 2328–2334, doi:10.1021/acs.jpclett.9b00727.

[9] R. W. Boyd. **Nonlinear Optics**. Academic Press, Inc., Orlando, FL, USA, 3rd edition, 2008.

[10] Y. R. Shen. **Fundamentals of Sum-Frequency Spectroscopy**. Cambridge University Press, University Printing House, Cambridge CB28BS, UK, 2016.

[11] E. Backus, J. Schaefer, and M. Bonn. *The mineral/water interface probed with nonlinear optical spectroscopy*. **Angew. Chem. Int. Ed. Engl.**, 2020, 60, 10482–10501, doi:10.1002/anie.202003085.

[12] S. M. Piontek and E. Borguet. *Vibrational dynamics at aqueous-mineral interfaces*. **J. Phys. Chem. C**, 2022, 126, 2307–2324, doi:10.1021/acs.jpcc.1c08563.

[13] M. Sparnaay. **The Electrical Double Layer**. Pergamon Press, Oxford, 1972.

[14] H.-J. Butt, K. Graf, and M. Kappl. **Physics and Chemistry of Interfaces**. Wiley-VCH, Weinheim, 2003.

[15] G. Gonella, E. H. G. Backus, Y. Nagata, D. J. Bonthuis, P. Loche, A. Schlaich, R. R. Netz, A. Kühnle, I. T. McCrum, M. T. M. Koper, M. Wolf, B. Winter, G. Meijer, R. K. Campen, and M. Bonn. *Water at charged interfaces*. **Nat Rev Chem**, 2021, 5, 466–485, doi:10.1038/s41570-021-00293-2.

[16] Q. Du, E. Freysz, and Y. R. Shen. *Vibrational spectra of water molecules at quartz/water interfaces*. **Phys. Rev. Lett.**, 1994, 72, 238–241, doi:10.1103/PhysRevLett.72.238.

[17] V. Ostroverkhov, G. A. Waychunas, and Y. R. Shen. *Vibrational spectra of water at water/α-quartz (0001) interface*. **Chem. Phys. Lett.**, 2004, 386, 144 – 148, doi:10.1016/j.cplett.2004.01.047.

[18] V. Ostroverkhov, G. A. Waychunas, and Y. R. Shen. *New information on water interfacial structure revealed by phase-sensitive surface spectroscopy*. **Phys. Rev. Lett.**, 2005, 94, 046102, doi:10.1103/PhysRevLett.94.046102.

[19] A. Myalitsin, S.-h. Urashima, S. Nihonyanagi, S. Yamaguchi, and T. Tahara. *Water structure at the buried silica/aqueous interface studied by heterodyne-detected vibrational sum-frequency generation*. **J. Phys. Chem. C**, 2016, 120, 9357–9363, doi:10.1021/acs.jpcc.6b03275.

[20] S. Dewan, M. S. Yeganeh, and E. Borguet. *Experimental correlation between interfacial water structure and mineral reactivity.* **J. Phys. Chem. Lett.**, 2013, 4, 1977–1982, doi:10.1021/jz4007417.

[21] E. L. DeWalt-Kerian, S. Kim, M. S. Azam, H. Zeng, Q. Liu, and J. M. Gibbs. *pH-dependent inversion of Hofmeister trends in the water structure of the electrical double layer*. **J. Phys. Chem. Lett.**, Jul 2017, 8, 2855–2861, doi:10.1021/acs.jpclett.7b01005.

[22] A. M. Darlington, T. A. Jarisz, E. L. DeWalt-Kerian, S. Roy, S. Kim, M. S. Azam, D. K. Hore, and J. M. Gibbs. *Separating the pH-dependent behavior of water in the Stern and diffuse layers with varying salt concentration*. **J. Phys. Chem. C**, 2017, 121, 20229–20241, doi:10.1021/acs.jpcc.7b03522.

[23] S.-h. Urashima, A. Myalitsin, S. Nihonyanagi, and T. Tahara. *The topmost water structure at a charged silica/aqueous interface revealed by heterodyne-detected vibrational sum frequency generation spectroscopy.* **J. Phys. Chem. Lett.**, 2018, 9, 4109–4114, doi:10.1021/acs.jpclett.8b01650.

[24] B. Rehl, M. Rashwan, E. L. DeWalt-Kerian, T. A. Jarisz, A. M. Darlington, D. K. Hore, and J. M. Gibbs. *New insights into $\chi^{(3)}$ measurements: Comparing nonresonant second harmonic generation and resonant sum frequency generation at the silica/aqueous electrolyte interface.* **J. Phys. Chem. C**, 2019, 123, 10991–11000, doi:10.1021/acs.jpcc.9b01300.

[25] A. Tuladhar, S. Dewan, S. Pezzotti, F. S. Brigiano, F. Creazzo, M.-P. Gaigeot, and E. Borguet. *Ions tune interfacial water structure and modulate hydrophobic interactions at silica surfaces*. **J. Am. Chem. Soc.**, 2020, 142, 6991–7000, doi:10.1021/jacs.9b13273.

[26] B. Rehl and J. M. Gibbs. *Role of ions on the surface-bound water structure at the silica/water interface: Identifying the spectral signature of stability.* **J. Phys. Chem. Lett.**, 2021, 12, 2854–2864, doi:10.1021/acs.jpclett.0c03565.

[27] K. C. Jena and D. K. Hore. *Variation of ionic strength reveals the interfacial water structure at a charged mineral surface.* **J. Phys. Chem. C**, Aug 2009, 113, 15364–15372, doi:10.1021/jp905475m.

[28] A. Rimola, D. Costa, M. Sodupe, J.-F. Lambert, and P. Ugliengo. *Silica surface features and their role in the adsorption of biomolecules: Computational modeling and experiments*. **Chem. Rev.**, 2013, 113, 4216–4313, doi:10.1021/cr3003054.

[29] O. Björneholm, M. H. Hansen, A. Hodgson, L.-M. Liu, D. T. Limmer, A. Michaelides, P. Pedevilla, J. Rossmeisl, H. Shen, G. Tocci, E. Tyrode, M.-M. Walz, J. Werner, and H. Bluhm. *Water at interfaces*. **Chem. Rev.**, 2016, 116, 7698–7726, doi:10.1021/acs.chemrev.6b00045.

[30] R. Wang, M. L. Klein, V. Carnevale, and E. Borguet. *Investigations of water/oxide interfaces by molecular dynamics simulations*. **WIREs Comput. Mol. Sci.**, 2021, 11, e1537, doi:10.1002/wcms.1537.

[31] S. Dewan, V. Carnevale, A. Bankura, A. Eftekhari-Bafrooei, G. Fiorin, M. L. Klein, and E. Borguet. *Structure of water at charged interfaces: A molecular dynamics study*. **Langmuir**, 2014, 30, 8056–8065, doi:10.1021/la5011055.

[32] O. Kroutil, Z. Chval, A. A. Skelton, and M. Předota. *Computer simulations of quartz (101)-water interface over a range of pH values*. **J. Phys. Chem. C**, 2015, 119, 9274–9286, doi:10.1021/acs.jpcc.5b00096.

[33] M. J. DelloStritto, J. D. Kubicki, and J. O. Sofo. *Effect of ions on H-bond structure and dynamics at the quartz(101)-water interface*. **Langmuir**, 2016, 32, 11353–11365, doi:10.1021/acs.langmuir.6b01719.

[34] M. Bouhadja and A. A. Skelton. *Dynamical properties of water and ions at the quartz (101)-water interface at a range of solution conditions: A classical molecular dynamics study*. **J. Phys. Chem. C**, 2018, 122, 1535–1546, doi:10.1021/acs.jpcc.7b08214.

[35] S.-H. Chen and S. J. Singer. *Molecular dynamics study of the electric double layer and nonlinear spectroscopy at the amorphous silica-water interface*. **J. Phys. Chem. B**, 2019, 123, 6364–6384, doi:10.1021/acs.jpcb.9b05871.

[36] M. F. Döpke and R. Hartkamp. *The importance of specifically adsorbed ions for electrokinetic phenomena: Bridging the gap between experiments and MD simulations*. **J. Chem. Phys.**, 2021, 154, 094701, doi:10.1063/5.0038161.

[37] A. Morita. **Theory of Sum Frequency Generation Spectroscopy**. Springer, Singapore, 2018.

[38] S. A. Hall, K. C. Jena, P. A. Covert, S. Roy, T. G. Trudeau, and D. K. Hore. *Molecular-level surface structure*

from nonlinear vibrational spectroscopy combined with simulations. **J. Phys. Chem. B**, 2014, 118, 5617–5636, doi:10.1021/jp412742u.

[39] T. Ishiyama, T. Imamura, and A. Morita. *Theoretical studies of structures and vibrational sum frequency generation spectra at aqueous interfaces*. **Chem. Rev.**, Sep 2014, 114, 8447–8470, doi:10.1021/cr4004133.

[40] M. F. Calegari Andrade, H.-Y. Ko, R. Car, and A. Selloni. *Structure, polarization, and sum frequency generation spectrum of interfacial water on anatase TiO_2*. **J. Phys. Chem. Lett.**, 2018, 9, 6716–6721, doi:10.1021/acs.jpclett.8b03103.

[41] F. Creazzo, D. R. Galimberti, S. Pezzotti, and M.-P. Gaigeot. *DFT-MD of the (110)-Co_3O_4 cobalt oxide semiconductor in contact with liquid water, preliminary chemical and physical insights into the electrochemical environment*. **J. Chem. Phys.**, 2019, 150, 041721, doi:10.1063/1.5053729.

[42] M. DelloStritto, S. M. Piontek, M. L. Klein, and E. Borguet. *Relating interfacial order to sum frequency generation with ab initio simulations of the aqueous Al_2O_3 (0001) and (11$\bar{2}$0) interfaces*. **J. Phys. Chem. C**, 2018, 122, 21284–21294, doi:10.1021/acs.jpcc.8b02809.

[43] T. Joutsuka, T. Hirano, M. Sprik, and A. Morita. *Effects of third-order susceptibility in sum frequency generation spectra: a molecular dynamics study in liquid water*. **Phys. Chem. Chem. Phys.**, 2018, 20, 3040–3053, doi:10.1039/C7CP01978E.

[44] T. Ohto, H. Tada, and Y. Nagata. *Structure and dynamics of water at water-graphene and water-hexagonal boron-nitride sheet interfaces revealed by ab initio sum-frequency generation spectroscopy.* **Phys. Chem. Chem. Phys.**, 2018, 20, 12979–12985, doi:10.1039/C8CP01351A.

[45] S. Pezzotti, D. R. Galimberti, Y. R. Shen, and M.-P. Gaigeot. *Structural definition of the BIL and DL: a new universal methodology to rationalize non-linear $\chi^{(2)}$ SFG signals at charged interfaces, including $\chi^{(3)}$ contributions*. **Phys. Chem. Chem. Phys.**, 2018, 20, 5190–5199, doi:10.1039/C7CP06110B.

[46] S. Pezzotti, R. D. Galimberti, R. Y. Shen, and M.-P. Gaigeot. *What the Diffuse Layer (DL) Reveals in Non-Linear SFG Spectroscopy*. **Minerals**, 2018, 8, 305, doi:10.3390/min8070305.

[47] S. Pezzotti, D. R. Galimberti, and M.-P. Gaigeot. *Deconvolution of BIL-SFG and DL-SFG spectroscopic signals reveals order/disorder of water at the elusive aqueous silica interface*. **Phys. Chem. Chem. Phys.**, 2019, 21, 22188–22202, doi:10.1039/C9CP02766A.

[48] K. Kim, S. Choi, Z. Zhang, L. Bai, S. Chung, and J. Jang. *Molecular features of hydration layers: Insights from simulation, microscopy, and spectroscopy*. **J. Phys. Chem. C**, 2022, 126, 8967–8977, doi:10.1021/acs.jpcc.2c01313.

[49] Y.-C. Wen, S. Zha, X. Liu, S. Yang, P. Guo, G. Shi, H. Fang, Y. R. Shen, and C. Tian. *Unveiling microscopic structures of charged water interfaces by surface-specific vibrational spectroscopy*. **Phys. Rev. Lett.**, 2016, 116, 016101, doi:10.1103/PhysRevLett.116.016101.

[50] A. Morita and J. T. Hynes. *A theoretical analysis of the sum frequency generation spectrum of the water surface. II. Time-dependent approach*. **J. Phys. Chem. B**, 2002, 106, 673–685, doi:10.1021/jp0133438.

[51] A. Morita. *Improved computation of sum frequency generation spectrum of the surface of water*. **J. Phys. Chem. B**, 2006, 110, 3158–3163, doi:10.1021/jp058155m.

[52] O. Kroutil, S. Pezzotti, M.-P. Gaigeot, and M. Předota. *Phase-sensitive vibrational SFG spectra from simple classical force field molecular dynamics simulations*. **J. Phys. Chem. C**, 2020, 124, 15253–15263, doi:10.1021/acs.jpcc.0c03576.

[53] K. S. Smirnov. *Structure and sum-frequency generation spectra of water on uncharged Q_4 silica surfaces: a molecular dynamics study*. **Phys. Chem. Chem. Phys.**, 2020, 22, 2033–2045, doi:10.1039/C9CP05765J.

[54] K. S. Smirnov. *Structure and sum-frequency generation spectra of water on neutral hydroxylated silica surfaces*. **Phys. Chem. Chem. Phys.**, 2021, 23, 6929 – 6949, doi:10.1039/D0CP06465C.

[55] N. H. de Leeuw, F. M. Higgins, and S. C. Parker. *Modeling the Surface Structure and Stability of α-Quartz*. **J. Phys. Chem. B**, 1999, 103, 1270–1277, doi:10.1021/jp983239z.

[56] L. Zhuravlev. *The surface chemistry of amorphous silica. Zhuravlev model*. **Colloid. Surface. A**, 2000, 173, 1–38, doi:10.1016/S0927-7757(00)00556-2.

[57] R. Rykart. **Quarz-Monographie: die Eigenheiten von Bergkristall, Rauchquarz, Amethyst, Chalcedon, Achat, Opal und anderen Varietäten**. Ott Verlag und Druckerei, Thun, 2nd edition, 1995.

[58] The shortest SiO^- – SiO^- distance was greater than 6.8 Å for the surface with the largest charge density.

[59] S. K. Milonjić. *Determination of surface ionization and complexation constants at colloidal silica/electrolyte interface*. **Colloids Surf.**, Apr 1987, 23, 301–312.

[60] R. Zerrouk, A. Foissy, R. Mercier, Y. Chevallier, and J.-C. Morawski. *Study of Ca^{2+}-induced silica coagulation by small angle scattering*. **J. Colloid Interface Sci.**, Oct 1990, 139, 20–29.

[61] M. A. Brown, A. Goel, and Z. Abbas. *Effect of electrolyte concentration on the Stern layer thickness at a charged interface*. **Angew. Chem. Int. Ed. Engl.**, 2016, 55, 3790–3794, doi:https://doi.org/10.1002/anie.201512025.

[62] Y. Wu, H. L. Tepper, and G. A. Voth. *Flexible simple point-charge water model with improved liquid-state properties*. **J. Chem. Phys.**, 2006, 124, 024503, doi:10.1063/1.2136877.

[63] F. S. Emami, V. Puddu, R. J. Berry, V. Varshney, S. V. Patwardhan, C. C. Perry, and H. Heinz. *Force field and a surface model database for silica to simulate interfacial properties in atomic resolution*. **Chem. Mater.**, 2014, 26, 2647–2658, doi:10.1021/cm500365c.

[64] This modification could not resolve the problem completely as an accidential deprotonation of water molecules was still observed in some simulations.

[65] I. S. Joung and T. E. Cheatham. *Determination of alkali and halide monovalent ion parameters for use in explicitly solvated biomolecular simulations*. **J. Phys. Chem. B**, 2008, 112, 9020–9041, doi:10.1021/jp8001614.

[66] K. C. Jena, P. A. Covert, and D. K. Hore. *The effect of salt on the water structure at a charged solid surface: Differentiating second- and third-order nonlinear contributions*. **J. Phys. Chem. Lett.**, May 2011, 2, 1056–1061, doi:10.1021/jz200251h.

[67] N. K. Kaliannan, A. Henao Aristizabal, H. Wiebeler, F. Zysk, T. Ohto, Y. Nagata, and T. D. Kuehne. *Impact of intermolecular vibrational coupling effects on the sum-frequency generation spectra of the water/air interface.* **Mol. Phys.**, 2020, 118, 1620358, doi:10.1080/00268976.2019.1620358.

[68] T. Ishiyama and K. Kitanaka. *Asymmetric hydrogen-bonding structure at a water/ice interface.* **J. Phys. Chem. C**, 2020, 124, 23287–23294, doi:10.1021/acs.jpcc.0c08173.

[69] P. E. Ohno, H.-f. Wang, and F. M. Geiger. *Second-order spectral lineshapes from charged interfaces*. **Nat. Commun.**, 2017, 8, 1032, doi:10.1038/s41467-017-01088-0.

[70] The analysis was carried out for the quartz/water interface with neat water and with the 0.25 M and 0.5 M NaCl solutions at pH 3, 6, 7 and 9. Additional points were obtained in simulations of system of smaller size (see ref. 54) at pH 3, 6, 7, and 8 for the 0.5 M salt concentration.

[71] B. Athokpam, S. G. Ramesh, and R. H. McKenzie. *Effect of hydrogen bonding on the infrared absorption intensity of oh stretch vibrations*. **Chem. Phys.**, 2017, 488-489, 43–54, doi:https://doi.org/10.1016/j.chemphys.2017.03.006.

[72] E. Ronca, L. Belpassi, and F. Tarantelli. *A quantitative view of charge transfer in the hydrogen bond: The water dimer case*. **ChemPhysChem**, 2014, 15, 2682–2687, doi:https://doi.org/10.1002/cphc.201402321.

[73] M. Pfeiffer-Laplaud and M.-P. Gaigeot. *Adsorption of singly charged ions at the hydroxylated (0001) α-quartz/water interface*. **J. Phys. Chem. C**, 2016, 120, 4866–4880, doi:10.1021/acs.jpcc.5b10947.

ELECTRONIC SUPPLEMENTARY INFORMATION

A molecular dynamics study of nonlinear spectra and structure of charged (101) quartz/water interface

Konstantin S. Smirnov

Univ. Lille, CNRS, UMR 8516 – LASIRe – Laboratoire Avancé de Spectroscopie pour les Interactions la Réactivité et l'Environnement, F-59000 Lille, France

S1 Computational details

S1.1 Nonbonded interatomic interaction potentials.

The nonbonded interatomic interactions were described by the sum of Lennard–Jones (12–6) and electrostatic potentials

$$E_{NB}^{(ij)}(r) = D_0^{(ij)}\left[\left(\frac{R_0^{(ij)}}{r}\right)^{12} - 2\left(\frac{R_0^{(ij)}}{r}\right)^{6}\right] + \frac{q_i q_j}{r} \tag{S1}$$

where i and j denote two atoms separated by a distance r, and R_0, D_0 and q are parameters whose values are given in Table S1.

Table S1: Parameters of interatomic potential functions (S1).

Atom[a]	Ow[b]	Hw[b]	Oh[c]	H[c]	Si[c]	Ob[c]	Six[c]	Ox[c,d]	Na[e]	Cl[e]
$q, \lvert e^- \rvert$	−0.82	+0.41	−0.675	+0.40	+1.1	−0.55	+0.725	−0.90	+1.0	−1.0
R_0, Å	3.5532	1.0	3.47	1.085	4.15	3.47	4.15	3.5532	2.424	5.422
D_0, kcal/mol	0.1554	0.0	0.122	0.015	0.093	0.054	0.093	0.1554	0.3526	0.0128

[a] Atom notation: Ow – water oxygen, Hw – water hydrogen, Oh – hydroxyl oxygen, H – hydroxyl hydrogen, Si – silicon, Ob – oxygen of siloxane bridges, Six – silicon of SiO^- groups, Ox – oxygen of SiO^- groups, Na – sodium, Cl – chlorine;
[b] ref. 1;
[c] ref. 2;
[d] vdW parameters were set to those of Ow kind, see Section 2 of the main article;
[e] ref. 3.

S1.2 Structural descriptors.

Structural organization of silica/water interface was characterized by a number of quantities. First, profiles of relative density $\rho^*(z)$ and of orientational order parameter $S_2(z)$ for the molecular dipole and the HH vector along the direction perpendicular to the surface (Cartesian z-axis) were computed. These quantities are given by

$$\rho^*(z) = \rho(z)/\rho_0 \tag{S2}$$

$$S_2(z) = \left\langle \frac{1}{N_z}\sum_{i=1}^{N_z} P_2(\cos\theta_i)\right\rangle, \tag{S3}$$

where ρ_0 is the density of bulk liquid water, $\cos\theta_i$ is the cosine between the vector and the z-axis, $P_2()$ is the second-order Legendre polynomial and N_z is a number of molecules in with CoM z-coordinate from

z to $z + \Delta z$. $S_2 = 1$ indicates the parallel-to-axis orientation, $S_2 = -0.5$ corresponds to a mean vector orientation perpendicular to the z-axis, and $S_2 = 0$ results from a random orientation of the vector with respect to the axis.

In addition to the $S_2(z)$ profiles, the orientation of water molecules in the interfacial region was described with a joint probability density distribution $P(u_1, u_2, \mathcal{Z})$ defined as[4]

$$P(u_1, u_2, \mathcal{Z}) = \frac{1}{N_{\mathcal{Z}}} \langle \sum_{i \in \mathcal{Z}} \delta(u_1 - \cos\phi_1^{(i)}) \cdot \delta(u_2 - \cos\phi_2^{(i)}) \rangle, \tag{S4}$$

where $\cos\phi_k^{(i)}$ ($k = 1, 2$) is the cosine of angle between the k-th OH bond vector of molecule i and the z-axis and the sum in (S4) runs over molecules in a region $\mathcal{Z}$. The normalization factor $N_{\mathcal{Z}}$ is given by

$$\int_{-1}^{1} P(u_1, u_2, \mathcal{Z})\, du_1 du_2 = 1. \tag{S5}$$

The analysis was perfomed for a quantity $\widetilde{P}(u_1, u_2, \mathcal{Z})$ given by

$$\widetilde{P}(u_1, u_2, \mathcal{Z}) = P(u_1, u_2, \mathcal{Z}) / P(u_1, u_2, \infty), \tag{S6}$$

wherea $P(u_1, u_2, \infty)$ stands for the distribution (S4) in an isotropic medium taken as bulk liquid water.

Network of intermolecular H-bonds was characterized by a joint probability density distribution $Q(r, u, \mathcal{Z})$ given by[5]

$$Q(r, u, \mathcal{Z}) = \langle \sum_{i \in \mathcal{Z}} \delta(r - R_{\mathrm{DA}}^{(i)}) \cdot \delta(u - \cos\psi^{(i)}) \rangle, \tag{S7}$$

where $R_{\mathrm{DA}}^{(i)}$ and $\cos\psi^{(i)}$ are the H-bond donor–acceptor (DA) distance and the cosine of angle between the DA vector and the z-axis, respectively (see Fig. 3 of ref. 6). The sum in (S7) runs over donor atoms with the z-coordinate lying in the region $\mathcal{Z}$. Hydrogen bonds were identified using geometric criteria[7].

S1.3 Nonlinear spectra.

Nonlinear spectra of interfacial water were obtained with the time correlation function (TCF) approach[8]. Following the approach, the pqr component of the resonant (R) part of the frequency-dependent second-order nonlinear susceptibility tensor $\boldsymbol{\chi}^{(2)}(\omega)$ is given by

$$\chi_{pqr}^{(2),R}(\omega) = \frac{i\omega}{k_B T} \int_0^{\infty} dt\, e^{i\omega t} \langle M_r(0) \cdot A_{pq}(t) \rangle, \tag{S8}$$

where M_r and A_{pq} are the r and pq elements of the system dipole $\mathbf{M}$ and polarizability $\mathbf{A}$, respectively. Experimentally, the most information is extracted from the analysis of sum-frequency generation spectra measured with the ssp polarization combination, that is the s- and p-polarized visible and infrared pulses, respectively, and the s-polarized sum-frequency radiation. The ssp spectrum in the work is obtained as the average of spectra of the xxz and yyz elements of the $\boldsymbol{\chi}^{(2),R}$ tensor. Hereafter, the corresponding quantity is denoted as $\chi_{\parallel\parallel\perp}^{(2),R}(\omega)$ (the $\parallel$ and $\perp$ symbols respectively designate the x or y, and z components).

The dipole moment $\mathbf{M}$ and polarizability tensor $\mathbf{A}$ of the liquid phase are obtained as

$$\mathbf{M} = \sum_m \boldsymbol{\mu}_m \tag{S9}$$

$$\mathbf{A} = \sum_m \boldsymbol{\alpha}_m, \tag{S10}$$

where $\boldsymbol{\mu}_m$ and $\boldsymbol{\alpha}_m$ stand for dipole moment and polarizability tensor of molecule m, respectively. Therefore, the TCF in (S8) corresponding to the $\chi^{(2),R}_{\parallel\parallel\perp}$ element of $\boldsymbol{\chi}^{(2),R}$ is given by[9–11]

$$C_{\parallel\parallel\perp}(t) = \frac{1}{2}\Big(\langle\sum_m \mu_{\perp,m}(0)\cdot a_{\parallel\parallel,m}(t)\rangle + \langle\sum_m \mu_{\perp,m}(0)\cdot\sum_{n\neq m} a_{\parallel\parallel,n}(t)\rangle\Big), \tag{S11}$$

where the first and second terms in (S11) are intramolecular (self) and intermolecular (cross) parts of the TCF, respectively. The calculation of the cross TCF in (S11) was restricted to molecules n within a sphere of 5.5 Å radius centered at the molecule m. A contribution of molecules of bulk region to the TCFs (S11) was attenuated[10–12] by multiplying the dipole $\mu_{\perp,m}(0)$ by a damping function $g(z_m)$

$$\mu'_{\perp,m}(0) = g(z_m(0))\mu_{\perp,m}(0), \tag{S12}$$

with $z_m(0)$ being the z-coordinate of the molecule m at $t = 0$; $\mu'_{\perp,m}(0)$ replaces $\mu_{\perp,m}(0)$ in (S11). The $g(z)$ function has the form

$$g(z) = \frac{1}{2}\mathrm{sign}(z)\big(\tanh(s(|z| - z_0)) + 1\big), \tag{S13}$$

where $g(z_0) = 1/2$ and parameter s determines the width of transition region. The value $s = 8.8$ Å^{-1} used in the work yields a width of 0.25 Å for the $0.1 - 0.9$ region. The `sign()` function in (S13) prevents the dipole $M_\perp$ from the cancellation because of the symmetry of the water slab with respect to $z = 0$. The TCF (S11) was computed on a length $L = 2048$ points (8.192 ps) and multiplied by a Hann apodization function of width $L/2$ prior to performing the Laplace-Fourier transform. The resulting spectra were smoothed by using a Gaussian filter with parameter σ equal to twice the frequency-step in the spectra (4.07 cm^{-1}). To estimate statistical uncertainty of the spectra calculation, a bootstrap sampling of 500 samples was performed for the dataset of 50 computed spectra. The uncertainties were subsequently used to obtain those of derived quantities.

S1.4 Spectrum of third-order susceptibility of bulk water.

The dipole $\boldsymbol{\mu}_m$ of molecule m can be written as

$$\boldsymbol{\mu}_m = \boldsymbol{\mu}^{(o)}_m + \boldsymbol{\mu}^{(i)}_m, \tag{S14}$$

where the first and the second term are the permanent and induced dipoles, respectively. Then, the TCF in (S8) can be rewritten as

$$C_{pqr}(t) = \langle M_r(0)\cdot A_{pq}(t)\rangle = \langle M^{(o)}_r(0)\cdot A_{pq}(t)\rangle + \langle M^{(i)}_r(0)\cdot A_{pq}(t)\rangle \tag{S15}$$

with $M^{(o)}_r$ and $M^{(i)}_r$ being the permanent (o) and induced (i) dipoles of the system, respectively, obtained by summing the corresponding molecular quantities (S9). If an electric field is applied to the system along an s-axis ($s = x, y, z$), the induced term in (S15) can be recast into

$$C^{(i)}_{pqr}(t) = \langle A_{rs}(0)\cdot A_{pq}(t)\rangle\, E_s \tag{S16}$$

where E_s is the field component along the axis. A $pqrs$ element of third-order susceptibility $\chi^{(3)}$ is given by

$$\chi^{(3)}_{pqrs} = \partial\chi^{(2)}_{pqr}/\partial E_s, \tag{S17}$$

and using (S8) and (S16), one readily obtains an expression for $\chi^{(3),R}_{pqrs}$ as

$$\chi^{(3),R}_{pqrs}(\omega) = \frac{i\omega}{k_B T}\int_0^\infty dt\, e^{i\omega t}\langle A_{rs}(0)\cdot A_{pq}(t)\rangle \tag{S18}$$

or with the use of (S10)

$$\chi^{(3),R}_{pqrs}(\omega) = \sum_m \left[\frac{i\omega}{k_B T}\int_0^\infty dt\, e^{i\omega t}\langle \alpha_{rs,m}(0)\cdot(\sum_n \alpha_{pq,n}(t))\rangle\right]. \tag{S19}$$

One can further split (S19) into the sum of self and cross terms, similarly to (S11). Note that the quantity in the square brackets in (S19) can be associated with the corresponding element of third-order molecular polarizability. It is worthy of noting that the above development is closely related to that in refs. 13–16, cf. eqn (1) of ref. 16.

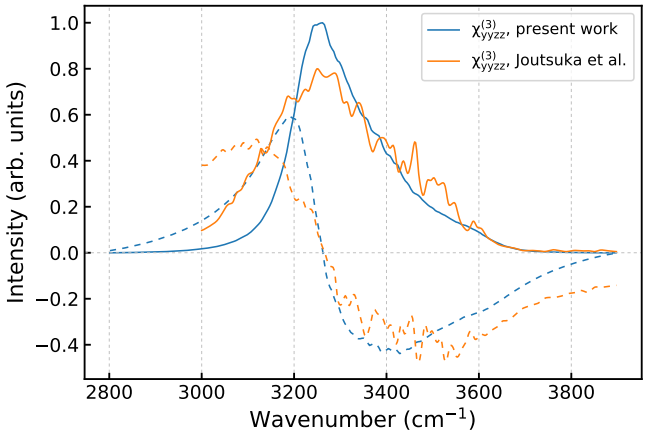

Figure S1: Calculated spectrum of the $yyzz$ element of $\chi^{(3),R}$ susceptibility of bulk water. Blue – present work, orange – digitized from Fig. 1a of ref. 17. Full and dashed lines denote the imaginary and real parts, respectively.

Figure S1 displays the spectrum of $\chi^{(3),R}_{yyzz}$ element for bulk liquid water computed with (S19) and compares it with the spectrum obtained in ref. 17. One sees a good agreement between the two spectra with differences readily explainable by different water models.

S2 Complementary results

S2.1 Vibrational spectra of isotopically diluted water.

Figure S2 shows the O-H bond stretching region of power spectrum of H atoms in an H_2O molecule diluted in bulk D_2O and of the atoms in normal water. The simulated system consisted of 500 molecules and represented liquid water at $\rho^* = 1$ and a temperature of 293 K. The strong similarity between the two spectra suggests a minor effect of intermolecular vibrational coupling on the spectrum.

S2.2 Breakdown of Im[$\chi^{(2),R}_{\parallel\parallel\perp}$] spectra of BIL at the 0.5 M ionic strength.

Figure S3 presents the breakdown of the Im[$\chi^{(2),R}_{\parallel\parallel\perp}$] spectra of BIL of quartz/water interface into the orientational and induced components for the 0.5 M NaCl solution.

S2.3 Orientation maps of OH bonds in BIL at the 0.5 M ionic strength

Figure S4 shows the $\widetilde{P}(u_1, u_2, \mathcal{Z})$ maps computed for water in BIL of the quartz/water interface for different pH values at the 0.5 M ionic strength. The patterns are essentially the same as for the 0.25 M electrolyte solution, cf Figure 12 of the main article.

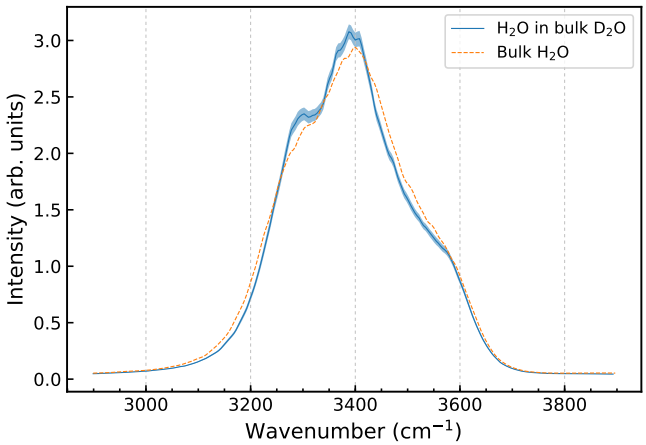

Figure S2: Power spectrum of H atoms of an H_2O molecule diluted in D_2O compared to the spectrum of H atoms in normal water. Colored area represents the standard error.

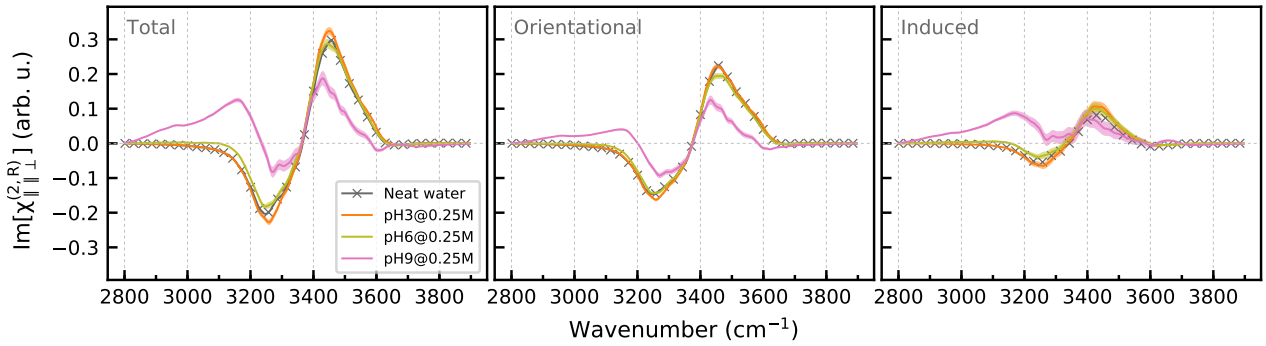

Figure S3: Breakdown of the $\mathrm{Im}[\chi^{(2),R}_{\parallel\parallel\perp}]$ spectra of BIL of (101) α-quartz/water interfaces into the orientational and induced components at the 0.5 M electrolyte concentration. The corresponding spectra of neutral surface/neat water interface are given for completeness. Colored areas represent the standard error.

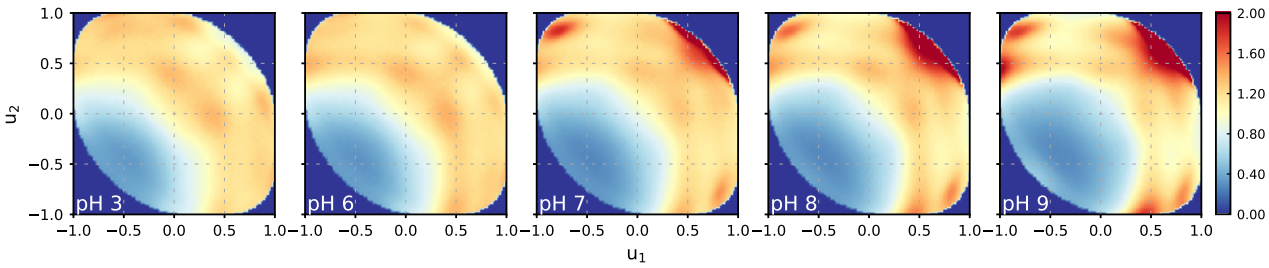

Figure S4: $\widetilde{P}(u_1, u_2, \mathcal{Z})$ maps for H_2O molecules in BIL of the (101) α-quartz/water interface at different pH values for the 0.5 M ionic strength.

S2.4 z-profiles of water structural characteristics in all systems

Profiles of the density ρ^* and order parameters S_2 along the z-axis for all studied systems are shown in Figure S5. Inspection of the data supports the conclusions presented in the main article.

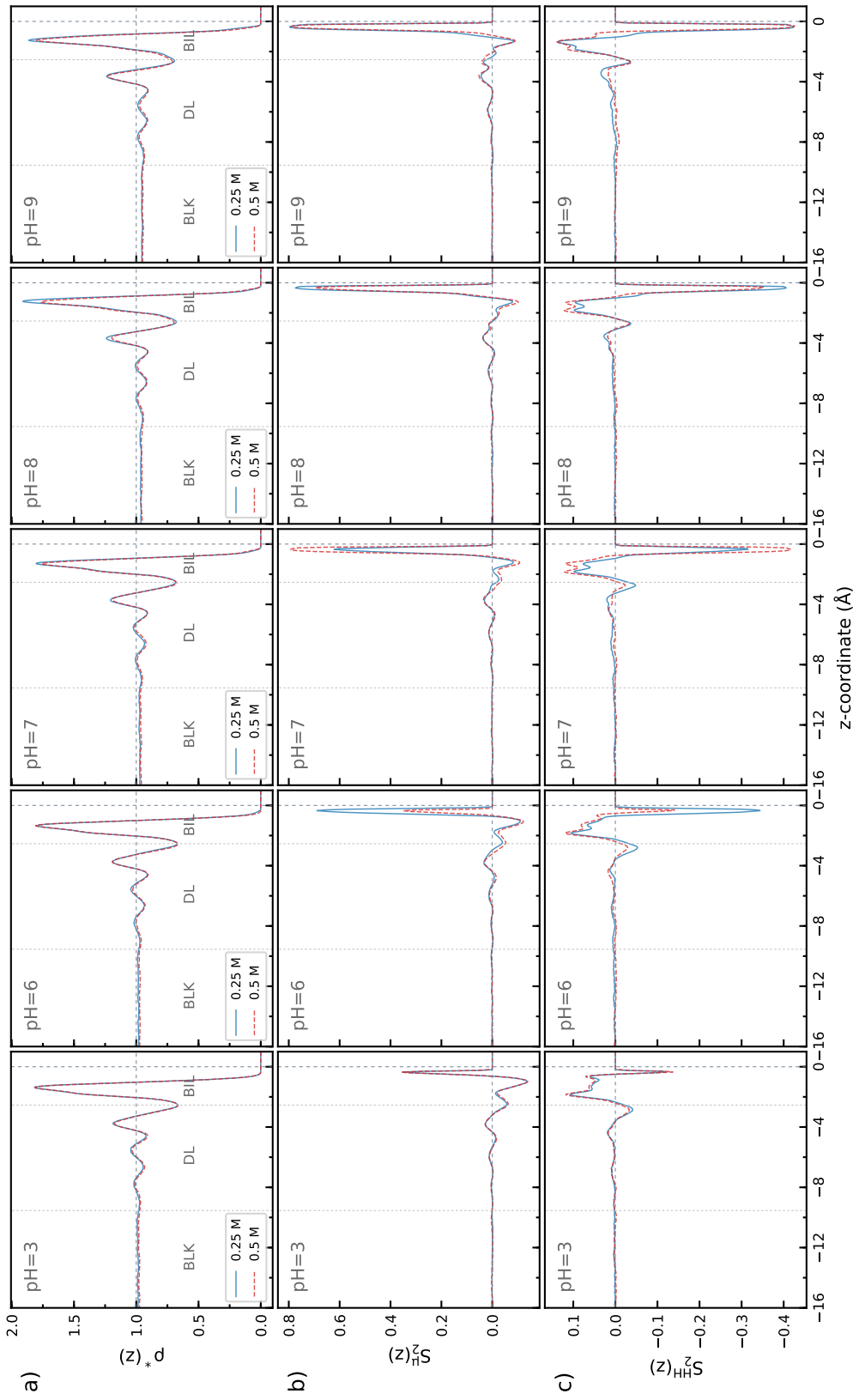

Figure S5: Axial profiles of the relative density $\rho^*(z)$ (a) and of the order parameters $S_2(z)$ for the dipole (b) and HH vector (c) of H_2O molecules at different pH values for the 0.25 M (full blue line) and 0.5 M (dashed red line) ionic strengths.

S2.5 z-profiles of ions distribution in all systems

Figure S6 presents the z-profiles of ion distribution in the interfacial region of all studied systems.

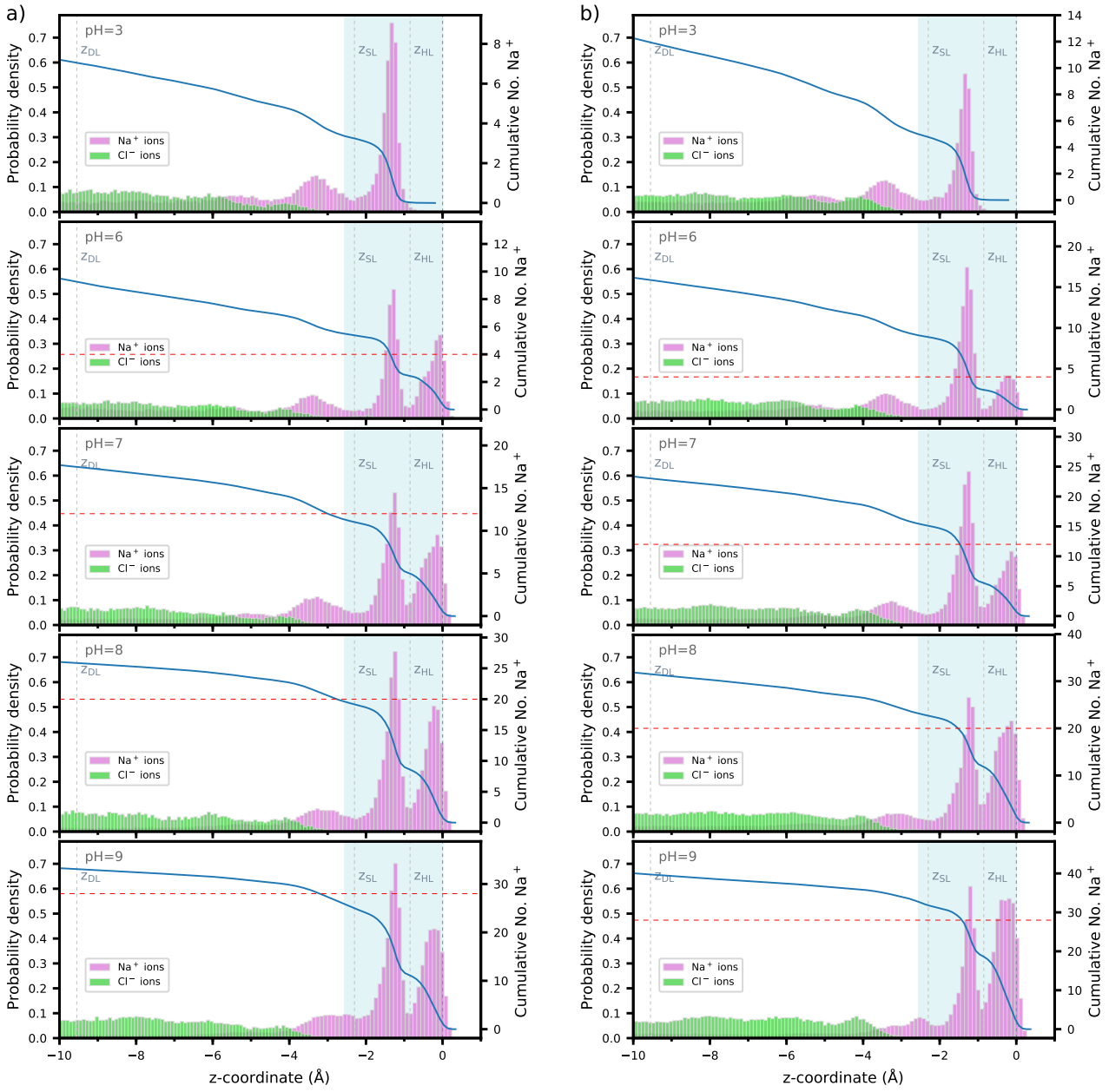

Figure S6: Histogram of ions distribution along the z-axis in the interfacial region at different pH values for the 0.25 M 3 (a) and 0.5 M (b) ionic strengths. The dashed vertical lines labeled z_{DL}, z_{SL} and z_{HL} indicate limits of the diffuse layer (DL), Stern layer (SL) and inner Helmholtz layer (HL), respectively. The shaded light blue zone denotes BIL, see Fig. S5 and the main article. The right-hand ordinate axis and blue line correspond to a cumulative number of cations as a function of distance from the surface. The red dashed line in the graphs indicates a number of cations needed to compensate the surface charge.

References

[1] Y. Wu, H. L. Tepper and G. A. Voth, *J. Chem. Phys.*, 2006, **124**, 024503.

[2] F. S. Emami, V. Puddu, R. J. Berry, V. Varshney, S. V. Patwardhan, C. C. Perry and H. Heinz, *Chem. Mater.*, 2014, **26**, 2647–2658.

[3] I. S. Joung and T. E. Cheatham, *J. Phys. Chem. B*, 2008, **112**, 9020–9041.

[4] A. P. Willard and D. Chandler, *J. Phys. Chem. B*, 2010, **114**, 1954–1958.

[5] S. Pezzotti, D. R. Galimberti, Y. R. Shen and M.-P. Gaigeot, *Phys. Chem. Chem. Phys.*, 2018, **20**, 5190–5199.

[6] K. S. Smirnov, *Phys. Chem. Chem. Phys.*, 2021, **23**, 6929 – 6949.

[7] D. Prada-Gracia, R. Shevchuk and F. Rao, *J. Chem. Phys.*, 2013, **139**, 084501.

[8] A. Morita and J. T. Hynes, *J. Phys. Chem. B*, 2002, **106**, 673–685.

[9] T. Ishiyama and A. Morita, *Chem. Phys. Lett.*, 2006, **431**, 78 – 82.

[10] T. Ishiyama and A. Morita, *J. Phys. Chem. C*, 2007, **111**, 738–748.

[11] Y. Nagata and S. Mukamel, *J. Am. Chem. Soc.*, 2011, **133**, 3276–3279.

[12] A. Morita, *J. Phys. Chem. B*, 2006, **110**, 3158–3163.

[13] R. W. Hellwarth, *Progress in Quantum Electronics*, 1977, **5**, 1–68.

[14] L. C. Geiger and B. M. Ladanyi, *Chem. Phys. Lett.*, 1989, **159**, 413–420.

[15] B. M. Ladanyi and Y. Q. Liang, *J. Chem. Phys.*, 1995, **103**, 6325–6332.

[16] S. Saito and I. Ohmine, *J. Chem. Phys.*, 1997, **106**, 4889–4893.

[17] T. Joutsuka, T. Hirano, M. Sprik and A. Morita, *Phys. Chem. Chem. Phys.*, 2018, **20**, 3040–3053.